

Type of the Paper (Article)

# Interface and Interphase in Polymer Nanocomposites with Bare and Core-Shell Metal Nanoparticles

Albert J. Power<sup>1,2,\*</sup>, Ioannis N. Remediakis<sup>3,4</sup> and Vagelis Harmandaris<sup>1,2,5,\*</sup>

<sup>1</sup> Department of Mathematics and Applied Mathematics, University of Crete, GR-71409, Heraklion, Crete, Greece; [ajpower@math.uoc.gr](mailto:ajpower@math.uoc.gr) (A.J.P.); [harman@uoc.gr](mailto:harman@uoc.gr) (V.H.)

<sup>2</sup> Institute of Applied and Computational Mathematics (IACM), Foundation for Research and Technology Hellas (FORTH), GR-71110 Heraklion, Crete, Greece; [ajpower@math.uoc.gr](mailto:ajpower@math.uoc.gr) (A.J.P.); [harman@uoc.gr](mailto:harman@uoc.gr) (V.H.)

<sup>3</sup> Department of Materials Science and Technology, University of Crete, GR-71003 Heraklion, Crete, Greece; [remed@materials.uoc.gr](mailto:remed@materials.uoc.gr) (I.N.R.)

<sup>4</sup> Institute of Electronic Structure and Laser, (IESL), Foundation for Research and Technology Hellas (FORTH), GR-71110 Heraklion, Crete, Greece; [remed@materials.uoc.gr](mailto:remed@materials.uoc.gr) (I.N.R.)

<sup>5</sup> Computation-based Science and Technology Research Center, The Cyprus Institute, Nicosia 2121, Cyprus; [harman@uoc.gr](mailto:harman@uoc.gr) (V.H.)

\* Correspondence: [ajpower@math.uoc.gr](mailto:ajpower@math.uoc.gr) (A.J.P.); [harman@uoc.gr](mailto:harman@uoc.gr) (V.H.); Tel.: +302810393735 (V.H.)

Received: date; Accepted: date; Published: date

**Abstract:** Metal nanoparticles are used to modify/enhance the properties of a polymer matrix for a broad range of applications in bio-nanotechnology. Here, we study the properties of polymer/gold nanoparticle (NP) nanocomposites through atomistic molecular dynamics, MD, simulations. We probe the structural, conformational and dynamical properties of polymer chains at the vicinity of a gold (Au) NP and a functionalized (core/shell) Au NP, and compare them against the behavior of bulk PE. The bare Au NPs were constructed via a systematic methodology starting from ab-initio calculations and an atomistic Wulff construction algorithm resulting in the crystal shape with the minimum surface energy. For the functionalized NPs the interactions between gold atoms and chemically adsorbed functional groups change their shape. As a model polymer matrix we consider polyethylene of different molecular lengths, from the oligomer to unentangled Rouse like systems. By computing the different properties the concept of the interface, and the interphase as well, in polymer nanocomposites with metal NPs are critically examined. Results concerning polymer density profiles, bond order parameter, segmental and terminal dynamics show clearly that the size of the interface / interphase, depends on the actual property under study. In addition, the anchored polymeric chains change the behavior/properties, and especially the chain density profile and the dynamics, of the polymer chain at the vicinity of the Au NP.

**Keywords:** molecular dynamics simulations; gold; nanoparticles; core-shell; grafted; structural and dynamical properties of polymers; polyethylene

## 1. Introduction

The study of polymer-based hybrid materials is a field of immense interest as it involves a broad spectrum of systems, applications, and spatiotemporal scales. On polymer/solid nanostructured systems in particular, the solid phase can strongly modify the properties of the entire hybrid system, such as its mechanical and electrical ones, as well as its dynamical/rheological behavior [1-7]. Therefore, the investigation of model polymer/solid interfacial systems, at the molecular level, is an intense research area, since such interfaces play a crucial role on the behavior of polymer-based systems with important technological applications, including for example polymer nanocomposites, polymer coatings, lubricants and thin films [8-12]. Examples include the modification of the electrochemical behavior [13] and the amelioration of the thermal degradation of the nanocomposites [14]. Moreover, there have been reports of enhancement of hardness, solvent

resistance and glossiness of nanocomposites [15]. The improvement of the tensile strengths of nanocomposite films [16] and the enhancement of the interfacial adhesion between nanoparticle and polymer matrix are also very important [17]. Furthermore, nanoparticles modify the mechanical properties of a polymer matrix [18, 19].

From the broad family of polymer nanocomposites (PNCs) here we focus on systems with (bare and core/shell) metal nanoparticles (NPs). Such systems have been used in the recent past in bio-nano-technology for biomedical utilization, including antibacterials [20], antimicrobials [21, 22], biosensors [23], cancer treatment [24] and biomedical tissue engineering [25, 26]. Their usage is also explored in other technological applications involving catalytic devices, in the textile industry and in food packaging [27-32]. In particular, polymer systems with dispersed gold (Au) NPs, or core/shell gold NPs, have been extensively studied due to their exceptional properties, such as biocompatibility, tunable conductivity and catalytic properties. Au nanoparticles of few nanometers (1 to 100nm) have a great surface/volume ratio and that enables their surface to be coated with many molecules (including therapeutics and targeting agents). Moreover, they are among the most stable of metal nanoparticles and they also provide a stable immobilization platform of the molecules while their reactivity is conserved. Their properties include colloidal stability and the ability to be conjugated with ease with biological molecules. Applications of polymer nanocomposites with Au NPs span many scientific fields, such as medicine [33] biotechnology [34], catalysis [35], and electronics [36]. In all these applications, the shape of Au nanoparticles has a key role in every aspect of their functionality, from sensing [37] and biolabeling applications [38] to plasmonics [39], photonics [40] and fuel cells [41]. Additional technological areas in which gold nanoparticles have been used include: the storage of energy [42], the delivery of molecules into cells [33, 43], use as a heat source [44], as sensors [45-47], labeling [48, 49], Light Emitting Diode (LED) applications [50], optical and electronic applications [39], drug delivery vehicles [51, 52] and in the field of catalysis [35, 53-55].

Besides experiments [56-64], molecular simulations have been used to study the properties of polymer-based complex materials [65-70], including atomistic molecular dynamics (MD) [3, 71-74], dynamic Monte Carlo simulations (MCMD) [75-77], self-consistent field theory (SCFT) and density functional theory (DFT) [78], dissipative particle dynamics (DPD) [79], coarse-grained MD simulations (CGMD) [80-83] and stochastic dynamics simulations [84].

It is now acknowledged that the behavior of polymer chains close to a polymer/solid interface is different from the behavior of the bulk [85-90]. For such systems, an interphase between the substrate and the bulk phase of the polymer is postulated, and the width of this interphase layer has been the focus of many studies. For example, it has been observed that segmental packing and orientation return to bulk values within just a few segment lengths from the surface and chain properties reached the bulk values after a few 1–2 times the radius of gyration  $R_g$  using atomistic and systematic coarse-grained models [86, 91], or bead–spring models [92, 93]. In addition, concerning the segmental dynamics of the macromolecules, relaxation times of segments at the vicinity of a solid surface strongly depend on the strength of the polymer/surface interactions [87, 94]. For polymer chains supported by a solid substrate the size of the interface or interphase depends on the actual property under study [86].

Furthermore, coarse-grained MD, Monte Carlo MD and atomistic MD simulations have been used to examine the viscoelastic behavior and the dispersion–aggregation transition of NPs in polymer nanocomposites with polymer-grafted nanoparticles systems [95-97], to compute the mean square displacement and the mean relaxation time of various intramolecular vectors [98], the structural properties and the mass density profiles of polymers brushes (grafted) [67, 76]. Moreover, several studies have investigated the polymer's structure, rheological properties and the shearing of the polymer between two gold surfaces, using MD simulations [99-101]. Finally, the mass density profiles, the mean square displacement, the polymers end to end distance and the radius of gyration on polymeric systems with gold nanoparticle have been examined through coarse-grained simulations and molecular dynamics simulation only on the interface [72].

Despite the above works, the study of the polymer/metal NP interface, and interphase as well, by predicting quantitatively the properties of polymer chains of specific polymer nanocomposites,

using realistic atomistic models for both polymer matrix and the Au NP is still a challenging problem. The aim goal of this work is to provide a detailed investigation of polymer nanocomposites with dispersed gold nanoparticles and core/shell gold nanoparticles, at the molecular level through detailed molecular dynamic simulations. As model polymer we consider polyethylene (PE). Bulk PE and PE-based nanocomposite materials are among the most widely used polymers in industry, and have been studied in depth during the recent years through experiments [102-104] and simulations [94, 105, 106]. The Au NPs and the functionalized Au NPs are made with Wulff construction derived directly from density functional theory (DFT) calculations [107, 108] in order to obtain model Au NPs with the minimum surface free energy, i.e. at thermodynamic equilibrium.

In the next section the model and the simulation method are described. Information for the analysis techniques that we have used and our results, divided in subsections, are presented in Section 3. Finally, a summary and the conclusions of the current study are presented in Section 4.

## 2. Model and Simulation Method

Here, we study PE nanocomposites with bare Au NPs and with functionalized, with short PE chains, (core/shell) NPs. The model gold nanoparticles, were generated using an atomistic Wulff construction algorithm [107, 108]. The grafting of the gold nanoparticles was accomplished by using anchored polyethylene chains. In all cases the temperature is 450K, above the melting temperature of PE. Ten (10) different model systems are considered, involving two different monodisperse PE matrices (Table 1); one consists of chains with 22 monomers (MW=310gr/mol) and the other one with 100 monomers (MW=1400gr/mol) [105, 106, 109]. Two different gold NPs with Wulff construction were modeled [107, 108]: one with diameter of 25 Å and one with 50 Å. Systems with the same polymer matrix but a different nanoparticle are also studied. Both of the grafted Au nanoparticles have a diameter of 5 nm and 53 grafted polyethylene chains. The first one has 20 monomers per chain and the other one 62 monomers per chain. The grafting density is 0.67 chains per square nm.

More details for all systems are presented in Table 1. Typical snapshots of the model PE/Au (bare and core/shell) NP systems are shown in Figure 1 and in Appendix Figure A1.

Name	Au NP Diameter	Au Atoms	Free PE Chains	Au/PE w/w%	Au/PE v/v%	Grafted PE Chains	Grafted PE mers/chain
PE100/Au2	25.1 Å	459	1200	4.9	0.2	-	-
PE100/Au5	50.2 Å	3101	1200	37.6	1.7	-	-
PE100/Au5/g20	50.4 Å	2461	1200	29.7	1.7	53	20
PE100/Au5/g62	50.4 Å	2461	1200	29.7	1.7	53	62
PE100	-	-	240	-	-	-	-
PE22/Au2	25.1 Å	459	5040	5.8	0.4	-	-
PE22/Au5	50.2 Å	3101	5040	38.8	1.6	-	-
PE22/Au5/g20	50.4 Å	2461	5040	30.8	1.6	53	20
PE22/Au5/g62	50.4 Å	2461	5040	30.8	1.6	53	62
PE22	-	-	420	-	-	-	-

**Table 1:** Details of the simulated model systems.

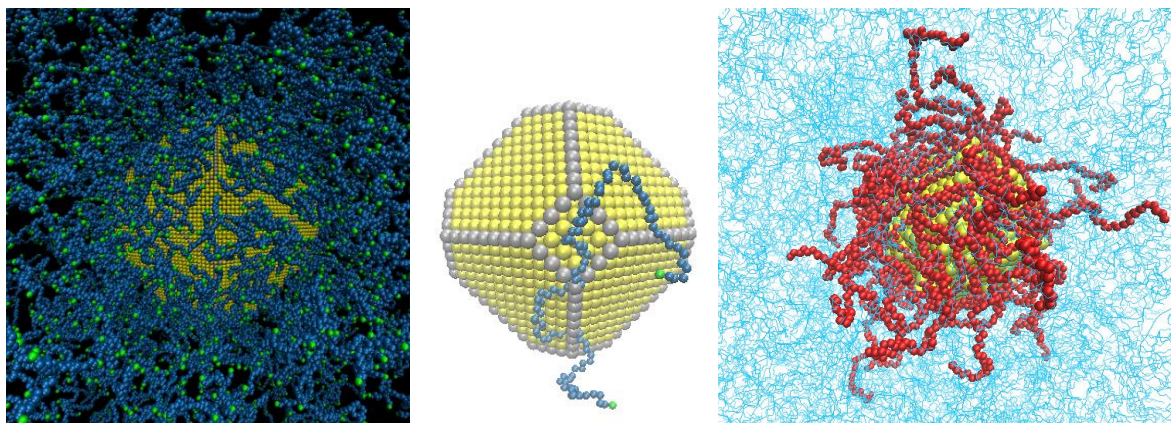


**Figure 1:** (Left) Snapshot from MD simulation of hybrid polyethylene/gold nanoparticle at 450K. Au nanoparticle (3101 atoms, diameter of 5.02 nm) and polyethylene (5040 chains, 22-mers per chain) are shown. In yellow is the Au, in blue are the CH<sub>2</sub> monomers and in green are the CH<sub>3</sub> monomers. (Center) Au nanoparticle (3101 atoms, diameter of 5.02 nm) and one chain of polyethylene (100-mers per chain) are shown. In yellow is the Au and in grey are the edges of Au nanoparticle, in blue are the CH<sub>2</sub> monomers and in green are the CH<sub>3</sub> monomers. (Right) Snapshot from MD simulation of hybrid polyethylene/grafted gold nanoparticle at 450K. Au nanoparticle (2461 atoms, diameter of 5.04 nm) and polyethylene (1200 chains, 100-mers per chain) are shown. In yellow is the Au and in grey are the edges of Au nanoparticle. In blue are the free CH<sub>2</sub> and the free CH<sub>3</sub> monomers. In red are the grafted CH<sub>2</sub> and CH<sub>3</sub> monomers.

Molecular Dynamics (MD) simulations were performed in the isothermal-isobaric (NPT) statistical ensemble, using the LAMMPS package [110]. The pressure was kept constant using Nosé Hoover barostat at  $P = 1$  atm. The Nosé Hoover thermostat was used to maintain the temperature at  $T = 450$  K. The integration time step was 1.0 fs and periodic boundary conditions were used in all three dimensions. For the representation of polyethylene a united atom model was used, where each methylene CH<sub>2</sub> and methyl CH<sub>3</sub> group was considered as a single Van der Waals interacting site. The polyethylene bonds and angles described by harmonic potential and the dihedrals by the OPLS force field (Appendix Table A1). For the Van der Waals interactions between the PE-PE (Appendix Table A2) we used a spherically truncated 6–12 Lennard–Jones potential with cutoff distance  $R_c = 10$  Å [105]. The first gold nanoparticle with Wulff construction has 459 atoms with 2.51 nm diameter and the second has 3101 atoms with 5.02 nm diameter [107, 108]. The interaction potential between the Au and PE (united) atoms was taken from the literature and is based on detailed DFT calculations [86]. For the core/shell Au NP systems [111], the minimum distance between the Au and the Sulfur is 1.7 Å. A harmonic potential is used to describe the thermal fluctuations associated with the Au-S-CH<sub>2</sub> angle. For the interactions between the S-PE (Appendix Table A2) we used a 6–12 Lennard–Jones potential with cutoff distance  $R_c = 10$  Å. For the S-CH<sub>2</sub>-CH<sub>2</sub>-CH<sub>2</sub> dihedral angle interactions the OPLS force field was used. The entire atomistic force field is given in Tables A1 and A2 of the Appendix. Tail corrections were applied to both energy and pressure. For the non-bonded interactions between PE-PE monomers, the Lorentz–Berthelot rules were used. The gold nanoparticles are frozen during the duration of the MD runs. This is not expected to be a crude assumption since the Au NPs are very stable under conditions (temperature and pressure) similar to those of the current simulations.

### 2.1. Shape of Au NPs

Gold nanoparticles can be found in nature in various shapes. Here we consider their “equilibrium” conditions, i.e. the shape with the minimum surface energy [53, 54, 108, 112]. At the thermodynamic limit, this is a polyhedron enclosed by faces of various ( $hkl$ ) crystal orientations such that the total surface energy, given by,

$$\sum_{hkl} A_{hkl} \gamma_{hkl} \quad (1)$$

is minimum.  $A_{hkl}$  is the total area of faces parallel to the  $(hkl)$  plane of the crystal and  $\gamma_{hkl}$  is the energy required to create a surface of unit area that is parallel to the  $(hkl)$  plane of the crystal and is the analog of the surface tension of liquids.

The Wulff construction has been used to predict equilibrium shapes in a variety of systems [113-115]. G. Wulff proposed that the shape that minimizes equation  $\sum_{hkl} A_{hkl} \gamma_{hkl}$

(1) is such that the distance of each face from the center is proportional to the surface tension of the respective  $(hkl)$  surface [115]:

$$d_{hkl} \sim \gamma_{hkl} \quad (2)$$

The equilibrium shapes of gold nanoparticles were predicted by linking extensive quantum-mechanical calculations, based on density functional theory (DFT), to Wulff constructions [107, 108]. In these calculations atomistic models of nanoparticles were constructed with diameters up to several tenths of a nanometer.

Different  $(hkl)$  planes bind differently to functional groups due to the presence of different atomic arrangements. As a result, the energies  $\gamma_{hkl}$  depend not only on the orientation  $(hkl)$  but also on the binding energy and the grafting density on the surface. The binding energies can be calculated using DFT [112]. This multi-scale scheme has been used to analyze shapes of nanoparticles of different materials, including SiO<sub>2</sub> [114], Au with adsorbed CO [108], Ag [116], and Pt in HCl [117].

Here, we use the nanoparticles generated with the method used in Ref.[107]. In that work, DFT and Wulff construction was used to calculate equilibrium shape of gold with adsorbed alkanethiols. The resulting shape resembled a deltoidal icositrahedron with twenty-four faces oriented towards  $(211)$ . In the absence of alkanethiols, the equilibrium shape was a truncated octahedron, with eight  $(111)$  faces and six  $(100)$  faces. Smaller nanoparticles usually have small deviations from the Wulff equilibrium shape as the smallest faces might have areas comparable to the atom cross-sections.

## 2.2. Generation and Equilibration of model systems

Generation and equilibration of model polymer nanocomposites is not a trivial issue. Below we describe shortly the procedure followed in order to obtain the model PE/Au nanocomposites:

- (a) First, in order to obtain initial PE/ grafted Au configurations, we added the anchors to the Au surface randomly by using a Monte Carlo algorithm in suitable positions according to the shape of the Au and taking in to account the absorption sites of sulfur in the DFT calculations for alkenethiols.
- (b) Second, we equilibrate the hybrid system through energy minimization and long simulation runs. Energy minimization of the core/shell system was performed followed by MD simulation runs up to 10 ns in the NVT ensemble. Third, the Au nanoparticle, grafted or not, was placed at a close distance (about 0.5 nm) to several well-equilibrated polymer samples [105].
- (c) The final step of our "equilibration protocol" involves the execution of long MD simulations, of the order of 30 ns were performed, during which the motion of the overall hybrid system was monitored. This time period is much longer than the time period required for the de-correlation of PE end-to-end vector [105].

Starting from the well equilibrated atomistic PE/Au configurations, production runs for times up to 100 ns were performed and several thousands of PE/Au NP configurations were saved. These configurations were used for the estimation of the properties of the entire hybrid systems and the detailed analysis of polyethylene/NP interfaces. Note, that the above methodology can be expanded to provide well equilibrated atomistic configurations of other polymer/core shell NP nanocomposites as well.

## 3. Results

### 3.1. Analysis Method

Our main goal is to study the spatial and dynamical heterogeneities of model hybrid polymer/nanoparticle systems in a detailed way at the molecular level. Therefore, properties of the polymer chains were examined as a function of the distance from the Au NP [94, 113]. The analysis presented here has been performed along radial distances from the center of mass of the gold NP (see Figure 2), by creating spherical shells of increasing radius (i.e., increasing distances from the Au NP), for each saved configuration.

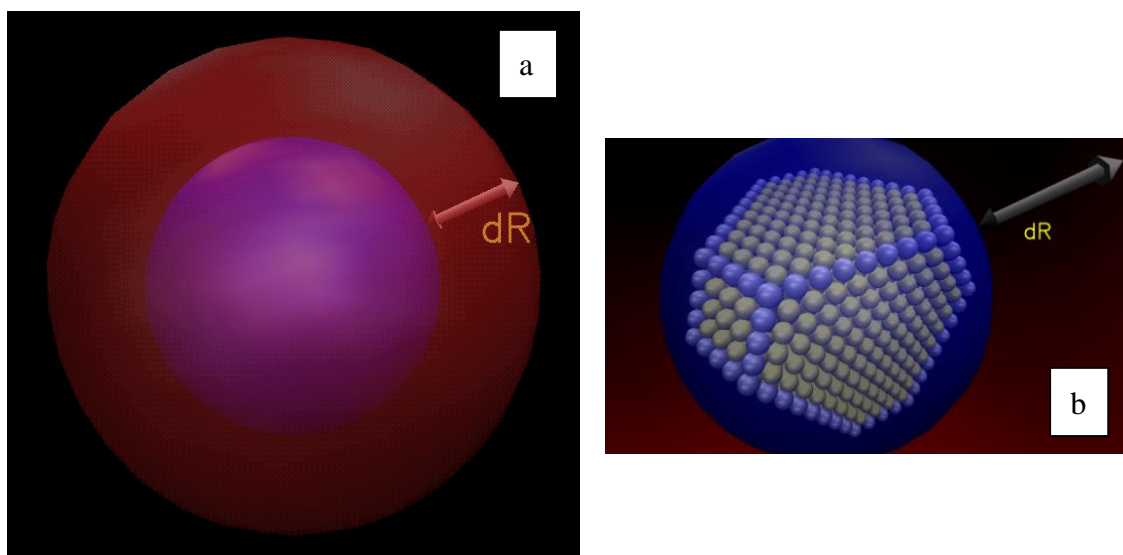


**Figure 2:** **a)** A sketch of the analysis scheme in spherical shells. **b)** Inside view of the Figure 2(a).

The mass density profiles were calculated according to the above discussed radial distance based analysis, using spherical shells of thickness equal to 1 Å. The same binning was used for the calculation of the second rank bond order parameter. Thicker spherical shells were used for the calculation of dynamical properties, of around 5 - 10 Å for both orientational and translational dynamics in the segmental level in order to improve statistics, whereas a 15 - 20 Å binning was used for the distribution of atoms according to their mean squared displacements in each shell. The choice of binning size (thickness of spherical shells) for the computation of each specific property is the result of an optimized balance between detailed information and improved statistics. Furthermore, for the calculation of the density of PE as a function of the distance from the nanoparticle, the mass (computed via the number) of PE atoms within each spherical shell was divided by its volume.

### 3.2. Structural Properties

#### 3.2.1. Density profiles

We start the analysis of the PE/Au model nanocomposites with the calculation of the mass monomer density profile of the polymer (PE) chains as a function of the distance from the gold NP. Average density profiles, which have been calculated for the center of mass of the monomers,  $\rho(r)$ , are presented in Figure 3 for all systems consisting of polyethylene matrices of 100mers per chain and in Appendix Figure A2 for all systems consisting of PE matrices of 22mers per chain.

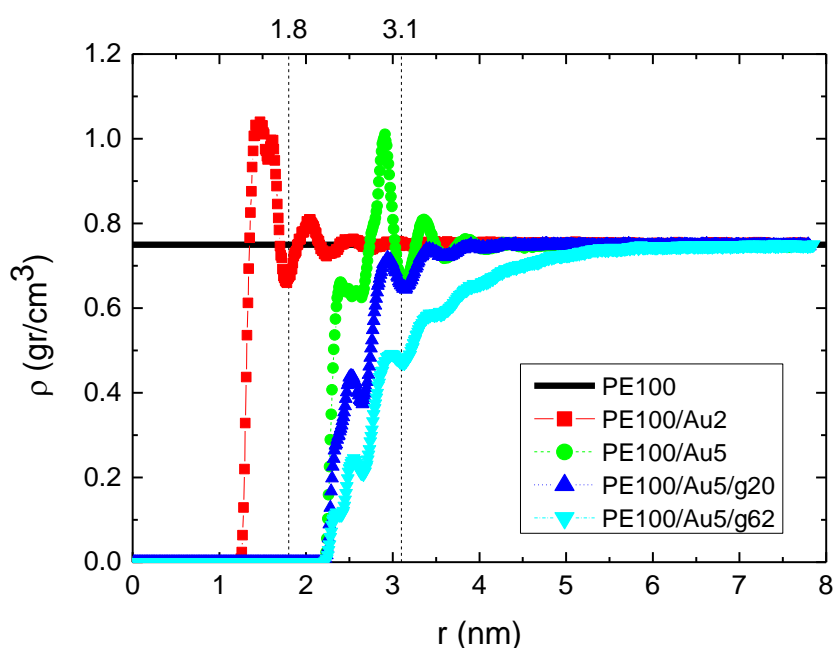


**Figure 3:** Mass monomer density profiles of polyethylene as a function of  $r$  (distance from the center of the gold NP) for the systems: PE100, PE100/Au2, PE100/Au5, PE100/Au5/g20 and PE100/Au5/g62.

In Figure 3, the polymer mass at each spherical shell has been divided by the total volume of the shell. Far from the Au NP, all curves reach/approach the bulk density value ( $\rho=0.75\text{gr/cm}^3$ ), though at different distances due to the different Au NP sizes. PE100/Au2 and PE100/Au5 systems exhibit the same behavior: a peak of rather similar height (but larger than the bulk value) is observed at a distance/radius of about 1.3 nm and 1.8 nm respectively, which denotes the attraction of the polymer atoms from the gold NP at short distances, due to vdW forces, while at longer distances the bulk density is attained. In the core/shell Au NP systems (PE100/Au5/g20 and PE100/Au5/g62), only few polyethylene chains can penetrate the anchors and reach the gold surface. We observe a similar behavior for the systems consisting of PE matrices of 22mers per chain although in this case the average density is lower than that of the systems consisting of PE matrices of 100mers per chain.

For the core/shell NP systems, the density profile can be decomposed to free polyethylene chains and grafted polyethylene chains. In Figure 4, the total PE density profiles is shown as well as its decomposition in “free” and “grafted” chains. We observe that the density values for the free polyethylene chains are lower than the corresponding bulk value close to the surface due to the nanoparticle’s anchors, which do not allow the interpenetration. However, the NP with short anchors allows more free PE chains to reach close to the surface compared to the case of long anchors NP. On the other hand for the grafted polyethylene chains (i.e., PE100/Au5/g20 and PE100/Au5/g62 systems) we observe a peak close to the Au NP due to the attraction from the surface. This peak is more pronounced for the case of PE100/Au5/g62 system due to the longer anchors. Moreover, the extension of anchors is up to 35 Å and up to 55 Å for the PE100/Au5/g20 and PE100/Au5/g62 systems respectively. Therefore, the corresponding bulk values are attained at these distances, as is observed in the density profiles of the total density curves (sum of free and grafted polyethylene chains). A similar behavior is observed for the PE22/Au2, PE22/Au5, PE22/Au5/g20 and PE22/Au5/g62 systems however in this case the average density is lower than that of the systems consisting of PE matrices of 100mers per chain.

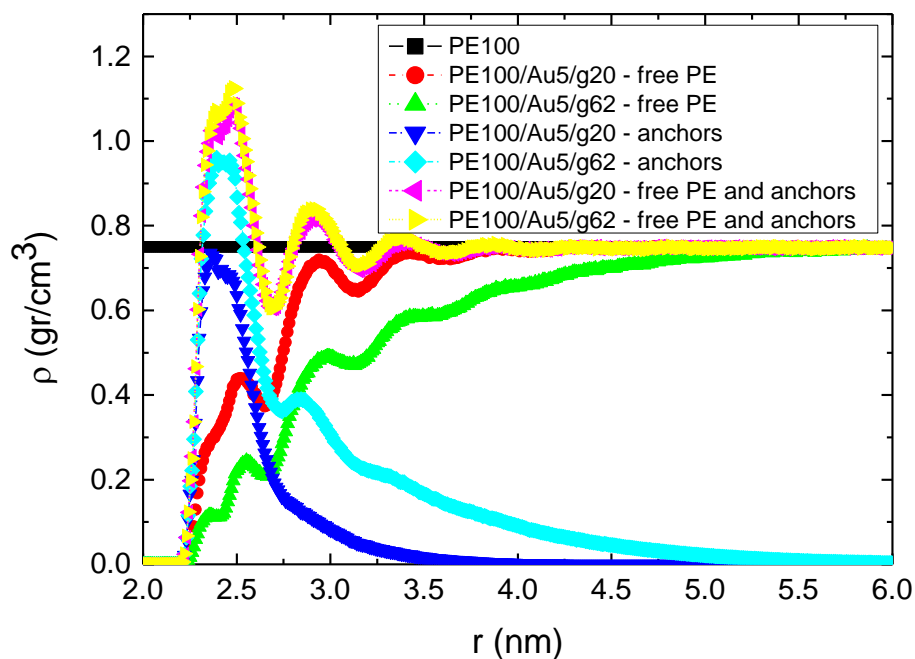


**Figure 4:** Mass monomer density profiles of polyethylene as a function of  $r$  (distance from the center of the gold NP) for the PE100/Au5/g20 and PE100/Au5/g62 systems. The density profile was decomposed to free polyethylene chains and grafted polyethylene chains.

### 3.2.2. Structure of PE chains

In the following we examine the orientation of the polymer chains close to the gold NP in the segmental level through the  $v^{1-3}$  vector which connects two non-consecutive carbon atoms. This is quantified via the second rank bond order parameter [12, 118] defined as:

$$P_2(\cos\theta) = \frac{3}{2} \langle \cos^2\theta \rangle - \frac{1}{2} \quad (3)$$

where  $\theta$  is the angle between the vector, which is defined along the molecule (here the  $v^{1-3}$  one) and the radial distance from the center of gold NP.  $P_2(\cos\theta)$  limiting values of  $-0.5$ ,  $0.0$ , and  $1.0$  correspond to perfectly parallel, random, and perpendicular vector orientations relative to the Au NP, respectively.

The bond order parameter of  $v^{1-3}$  for all systems with PE matrices consisting of 100mers per chain is depicted in Figure 5. In all cases there is an obvious tendency of the segments of the polymer chain for an almost parallel to the gold NP orientation at short distances which is gradually randomized the further the distance. There is a decrease of the bond order parameter of the PE segments closest to the Au NP and the minimum values are about  $-0.4$  for all hybrid systems. The same behavior is observed for the other model systems studied here as well.

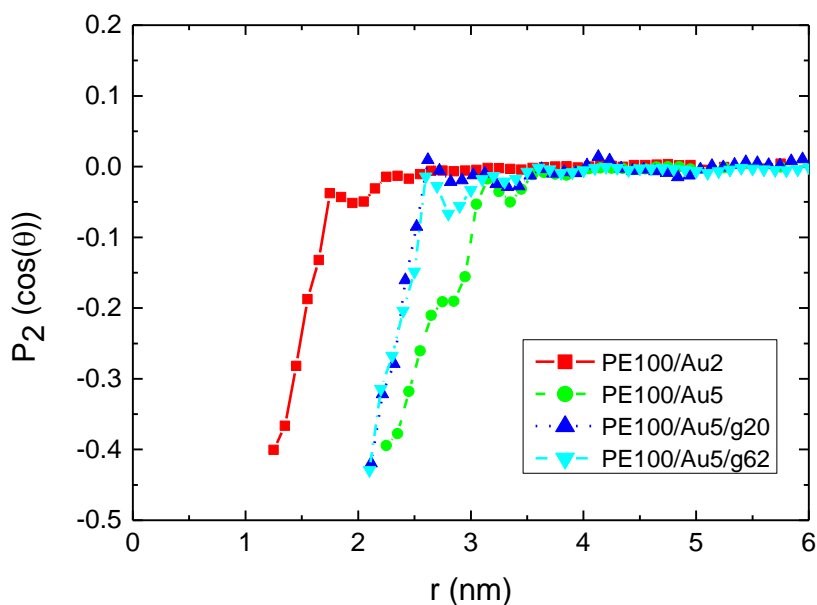


**Figure 5:** Second rank bond order parameter  $P_2(\cos(\theta))$  of polyethylene for  $v^{1-3}$  vector as a function of  $r$  distance (distance from the center of the Au NP) for all polymer/gold nanoparticle systems with PE matrices consisting of 100mers per chain.

A further analysis of the PE chain conformations at the segmental level is based on the calculation of the distribution of the torsional (dihedral) angles,  $P_{dih}$ , in different distances from a gold NP. This is of particular importance since for PE the distribution of its (backbone) dihedral angle is critical for the determination of its overall chain conformation. Results about the dihedral angle distributions of the PE chains are shown in Figure 6a for the PE100/Au2 system (“trans” corresponds to  $0^\circ$ , “gauche-” and “gauche+” to  $-60^\circ$  and  $+60^\circ$  respectively and “cis” to  $180^\circ$  degrees). For the first adsorption layer, defined via the first minimum in the density profile (0-30 Å, see Figure 3), a non-negligible enhancement of the trans states with a consequent reduction of the gauche ones is observed for PE22/Au2, PE22/Au5, PE100/Au2 and PE100/Au5 systems compared to the bulk case (Figure 6b). This observation reflects the more ordered PE chains close to the gold NP. Enhancement of “trans” population would be expected to affect the crystallinity of PE chains as well as the mechanical properties of the hybrid system. Such a behavior has been observed for PE adsorbed on planar carbon-based surfaces, such as graphite or graphene, where the structure of PE commensurate to the underlying crystal structure of the substrate [3, 94, 119, 120]. Here the enhancement of trans population is rather weak.

Concerning the system with the functionalized Au NPs (PE22/Au5/g20, PE22/Au5/g62, PE100/Au5/g20 and PE100/Au5/g62) no differentiation in the torsional angle distributions is detected. Short anchors as in PE100/Au5/g20 and PE22/Au5/g20 systems are enough to make the dihedral distribution peak to disappear. For the most distant adsorption layer (i.e., bulk region), the curves are completely identical to each other and to the corresponding bulk one.

In addition, the radius of gyration ( $R_g$ ) for the PE was calculated and found approximately 6 Å in the systems consisting of 22 monomers per chain (Appendix Figure A3) and approximately 16 Å in the systems consisting of 100 monomers per chain (Appendix Figure A4).

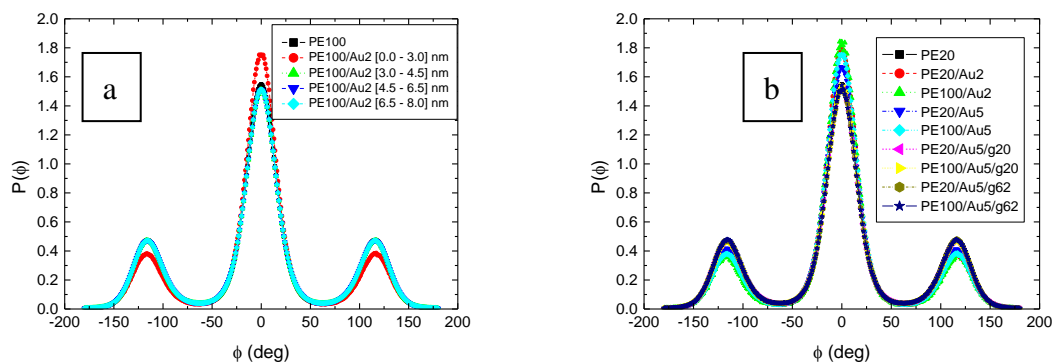


**Figure 6:** (a) Torsional angles distribution of PE chains for various distances from the center of the gold NP for the PE100/Au2 system and the corresponding PE bulk curve. (b) Torsional angles distributions of all model systems for PE chains belonging in the first adsorbed layer, i.e. being closer to the Au NP. The corresponding curves for bulk PE are also shown.

### 3.3. Dynamical Properties

In this section we present data concerning the dynamical properties of polymer chains in the model nanocomposites with bare, and functionalized core/shell Au NPs. We perform the analysis by calculating corresponding quantities of PE chains, both as averages for the entire nanocomposite and as a function of distance from the PE/Au interface.

#### 3.3.1. Orientational Dynamics

First, we study the orientational dynamics at the terminal level, via the time autocorrelation function (ACF) of the second Legendre polynomial:

$$P_1(t) = \langle \cos\theta(t) \rangle \quad (4)$$

In more detail, we define the end to end,  $v^{e-e}$ , vector, which connects the first and last carbon atom of the chain, and  $\theta(t)$  is the angle of this vector at time  $t$  relative to its position at  $t = 0$ . Results for the autocorrelation function,  $P_1(t)$  at different radial adsorption layers are presented in Figure 7 for the hybrid PE100/Au5 system and the comparison with PE22/Au5 system in Appendix Figure A5. Corresponding data for a bulk PE system are shown in these figures as well. Note that for these calculations we monitor the position of each vector only for the time period it belongs to the corresponding analysis regime. It is clear that in all systems slower PE chain dynamics at the vicinity of the Au nanoparticles is shown. In particular, PE chains in the first adsorption layers show much slower terminal dynamics compared to the bulk one. A faster decorrelation is then observed moving away from the surface up to a specific distance, while beyond this all curves coincide. We've also calculated the average value of the ACF for the entire system, which is almost identical with the bulk's one.

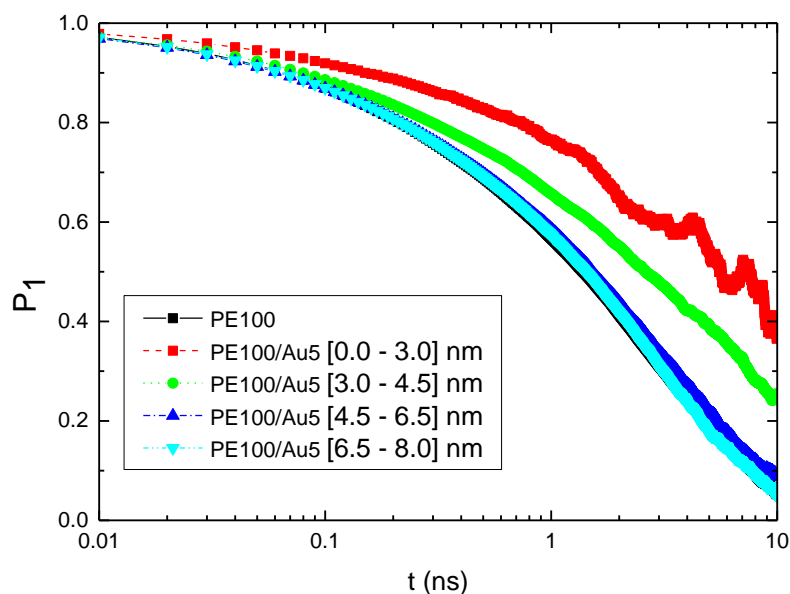


**Figure 7:** Time autocorrelation function (ACF) of bond order parameter  $P_1(t)$  as a function of time for the characteristic vector  $v^{e-e}$  of polyethylene for PE100/Au5 system. PE chains are analyzed across various shells from the Au NP.

The effect of the PE/gold nanoparticle interface on the PE terminal dynamics of each system can be further quantified by computing the corresponding chain relaxation times, through proper fits of curves shown in Figure 7, with a Kohlrausch–Williams–Watts (KWW) stretch exponential function [121] of the form:

$$P_1(t) = A \exp \left[ - \left( \frac{t}{\tau_{KWW}} \right)^\beta \right] \quad (5)$$

where,  $A$  is a pre-exponential factor which takes into account relaxation processes at very short times (e.g., bond vibrations and angle librations),  $\tau_{KWW}$  is the KWW relaxation time and  $\beta$  the stretch exponent, which describes the broadness of the distribution of the relaxation times (*i.e.*, the deviation from the ideal Debye behavior  $\beta = 1$ ). Then, the relaxation time,  $\tau_{end-end}$ , is calculated as the integral of the KWW curves through:

$$\tau_{end-end} = \frac{\tau_{KWW}}{\beta} \Gamma \left( \frac{1}{\beta} \right) \quad (6)$$

where  $\Gamma(\cdot)$  is the gamma function.

The results of the above analysis for both the relaxation time  $\tau_{end-end}$  and the  $\beta$  exponent for PE chains of all the simulated systems are presented in Figure 8 and Figure 9. Bulk values are also shown in these figures. It is clear that the PE chains which are very close to the Au NP, have much slower orientational dynamics (longer terminal relaxation time  $\tau_{end-end}$ ) and  $\tau_{end-end}$  is about 2-10 times longer than the bulk one. As expected polymer chains become more mobile as their distance from the gold nanoparticle increases, reaching a plateau, bulk-like regime, at distances of about 1.0–1.5 nm away from the Au NP. In addition,  $\beta$ -exponent values of PE chains are smaller than the bulk value ( $\sim 0.89$ ), the black line shown in Figure 9, at the majority of all distances. The latter indicates a broader distribution of the polymer terminal dynamics, compared to the bulk one. Furthermore as was expected, the 100mers PE systems have much slower relaxation times in comparison to those of the 22mers PE systems (Appendix Figures A6-A11).

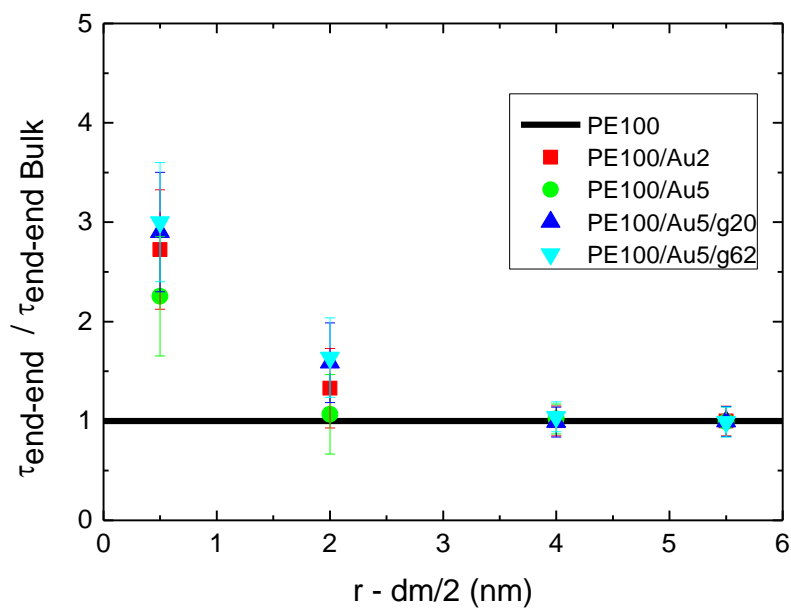


**Figure 8:** Relaxation time,  $\tau_{\text{end-end}} / \tau_{\text{end-end Bulk}}$  of  $v^{e-e}$  characteristic vector based on  $P_1(t)$  time autocorrelation as a function of  $r$  (distance from the center of the Au NP) minus the half diameter of the NP for all systems with PE matrices consisting of 100mers per chain.

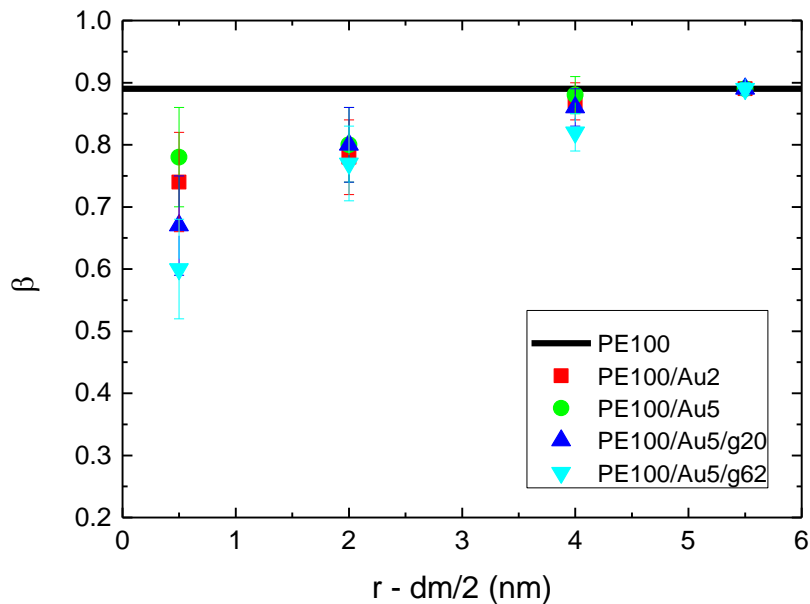


**Figure 9:** The stretch exponent  $\beta$ , as extracted from the fit with KWW functions, of  $v^{e-e}$  characteristic vector based on  $P_1(t)$  time autocorrelation as a function of  $r$  (distance from the center of the Au NP) minus the half diameter of the NP for all systems with PE matrices consisting of 100mers per chain. Black lines represent  $\beta$  values of bulk PE.

### 3.3.2. Translational Dynamics

In the next stage, we examine the translational segmental dynamics of PE chains. To distinguish translational dynamics for different layers we have calculated the average segmental mean-square displacement (MSD) defined as:

$$\Delta R_j(\tau) = \langle [r_i(t + \tau) - r_i(t)]^2 \rangle \quad (7)$$

where  $j$  is a specific radial region,  $i$  is a particular segment (CH<sub>2</sub> or CH<sub>3</sub> group here) within region  $j$ ,  $r_i(t)$  and  $r_i(t + \tau)$  are the coordinate vectors of segment  $i$  at time  $t$  and  $t + \tau$ , respectively, whereas brackets  $\langle \rangle$  denote statistical average. Note, that in the analysis used here a segment  $i$  contributes to the above average MSD for a given time interval  $\tau$  and for a radial region  $j$ , if and only if it was constantly present in that region in the entire course of time  $\tau$ . In Figure 10 data concerning  $\Delta R_j(\tau)$  for all (radial) adsorption layers for the PE100/Au5/g62 system is shown. The terminal dynamics of the polymer atoms that are closer to the Au NP atoms (mainly in the first adsorption layer) is slower compared to the one of the atoms in the other layers. On the contrary, chains belonging to the other regimes, (above the second layer) exhibit rather similar dynamics, which is almost equal to the bulk one, the black line and the total average value of the entire system, the magenta line shown in Figure 10. All the simulated hybrid systems have a similar behavior. However, the PEs in PE22/Au2, PE22/Au5, PE22/Au5/g20 and PE22/Au5/g62 (see Appendix Figure A12) are faster than the equivalent systems with PE matrices consisting of 100mers per chain.

According to the Rouse model predictions [69]  $\Delta R_j(\tau) \propto t^{1/2}$ . Our calculations using the data for bulk PE (PE100 system) showed that the Rouse regime was well-attained for the linear bulk chains, as it has been shown also in previous works [122-124]. Concerning the different adsorption spherical shells we extracted exponents less than 1/2. Those exponents indicate the variation from the Rouse behavior which is more pronounced close to the Au NP. This attributed to the fact that there is attraction of the PE monomers from the Au NP and from the grafted polymers. Furthermore, according to our analysis method, we calculated the MSD for the hybrid systems as long as the segments were within the spherical shells. Therefore the time frame window is not enough to reach the Rouse regime for the PE monomers that are close to the surface of the Au NP.

The MSD,  $\Delta R_j(\tau)$  at the 1<sup>st</sup> adsorption spherical shell is presented in Figure 11 for all simulated systems with PE matrices consisting of 100mers per chain. We observe that the MSD,  $\Delta R_j(\tau)$  in all systems for the 1<sup>st</sup> adsorption shell is smaller than the corresponding bulk one.

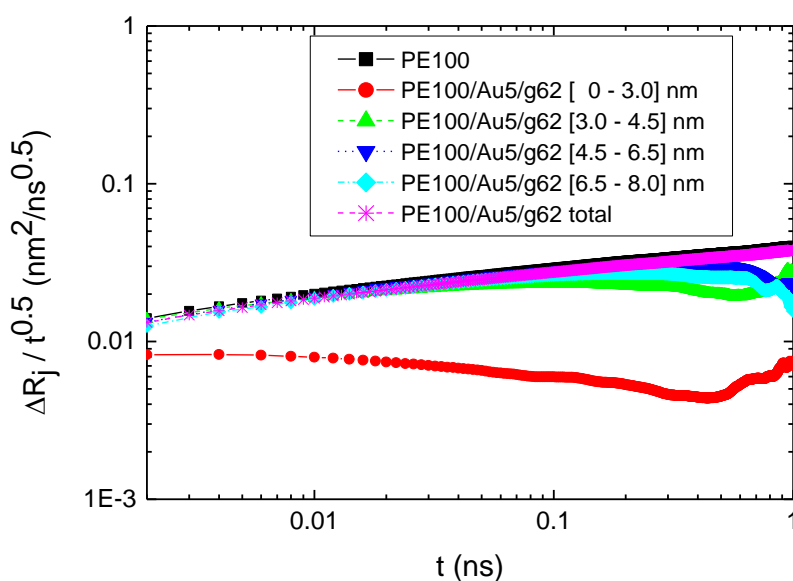


**Figure 10:** Segmental mean squared displacement for polyethylene chains along  $R$  (distance from the center of the gold NP) scaled with  $t^{0.5}$ ,  $\frac{\Delta R_j}{t^{0.5}}$ . Values for the PE100 and PE100/Au5/g62 systems, for various spherical shells and the total value of the entire system.

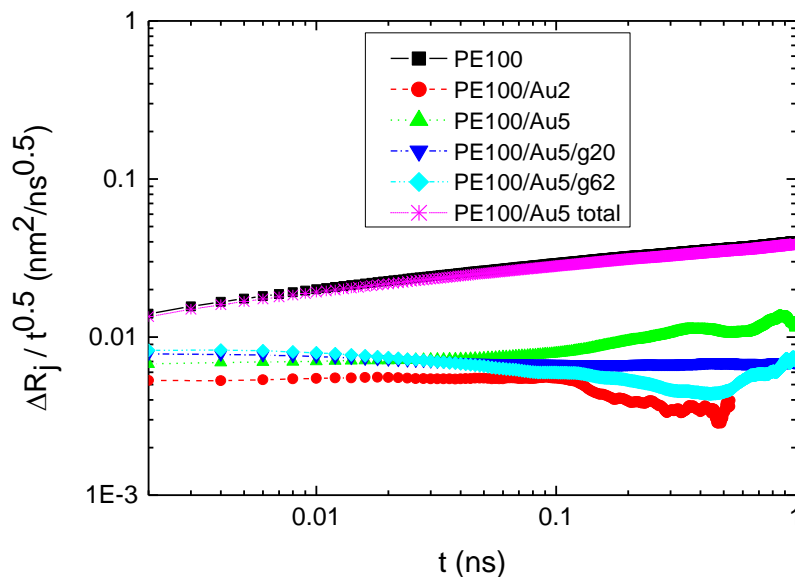


**Figure 11:** Segmental mean squared displacement for polyethylene chains along  $R$  (distance from the center of the gold NP) scaled with  $t^{0.5}$ ,  $\frac{\Delta R_j}{t^{0.5}}$ . Values for the PE100, PE100/Au2, PE100/Au5, PE100/Au5/g20 and PE100/Au5/g62 systems, for the first adsorption spherical shell of each system and the total value of the entire PE100/Au5 system.

#### 4. Discussion and Conclusions

The term of interphase, a three-dimensional zone, is used to indicate a regime between two phases where properties are gradually changing from one phase to another, in contrast to the more traditional two-dimensional like “interface” one. For polymer nanocomposites the properties of polymer chains at the interphase are of paramount importance for the performance of these composite systems. Here, we studied, through detailed atomistic MD simulations, polymer nanocomposites with bare and core/shell metal (gold) NPs. Polyethylene chains of different molecular weights, consisting of 20 monomers per chain and 100 monomers per chain are used as a model polymer matrix. Au NPs were constructed in their equilibrium Wulff shape (minimum surface free energy) via DFT calculations. Two different Au NP sizes of 2.5nm and 5.0nm diameter were modeled. For the functionalized NPs grafted anchors of 20 and 62 monomers per anchor chain were considered. Various structural and dynamical properties of the PE chains were computed to examine the structure and the width of the PE/Au NP interphase.

The behavior of polyethylene is affected by the spatial heterogeneities induced by the presence of PE/Au NP interfaces. The average properties of the hybrid systems are, as expected, close to those of the bulk PE, due to the rather low concentration of the NPs. However, structural and dynamical properties of the polymers show dramatic changes near the Au NPs. A detailed analysis was proposed based on averaging over atoms (or chains) within radial spherical shells equidistant from the center of the gold NP which allows us to examine the way that spatial heterogeneities are related to structural and dynamical features of the hybrid system as a function of distance from the polymer/gold nanoparticle interface.

From the analysis of the simulation it is clear that the width of the PE/Au NP interphase depends on the actual property under study. First, it is clear that at the vicinity of the bare Au NPs a dense layer of polymer atoms appears. Second, for the case of the core/shell NPs the anchors change polymer’s behavior/properties and especially the density profile. Moreover, the backbone vector of PE is oriented parallel to the gold surface. Furthermore, dynamics become slower close to the Au NP

and terminal relaxation time decreases with the distance from the Au NP. Finally, the examined polymer properties attain their bulk-like values far from the Au NP's surface, whereas as expected by increasing the molecular weight, the density (slightly) increases and the dynamics become slower.

In Table 2 we summarize the effect of interface on various properties. Results can be summarized as follows:

- Local **structural** and **conformational** features were analyzed at the level of both individual segments (atoms or bonds) and entire chains. The local monomer PE mass density near the gold surface exhibits a maximum due to the intermolecular PE/Au NP (adhesive) interaction. Chain segments show a tendency for an almost parallel to the Au NP orientation at short distances which is gradually randomized as one moves away from the interface. In addition, increase of "trans" population in the dihedral angle distribution at the PE/gold NP interface compared to the bulk one has been observed, which reflects the more ordered polymer chain structures.
- **Orientalional** relaxation of PE chains in the hybrid systems at the segmental and terminal level was quantified through the time autocorrelation function of the second Legendre polynomial. Qualitatively similar behavior was found for all systems: PE chains closer to the Au NP show much slower orientational dynamics (segmental relaxation time  $\tau_{\text{seg}}$  is about 10 times longer) compared to the bulk one. Faster  $P_2(t)$  decorrelation is observed moving away from the interface up to a specific distance, while beyond this, all curves coincide. In addition, broader distribution of the polymer orientational dynamics was found, compared to the bulk one (smaller  $\beta$ -exponent values).
- **Translational** segmental and center of masses dynamics of PE chains were examined through the calculation of the average mean-square displacement. PE chains closer to the Au NP are slower, compared to the bulk one, for all model hybrid systems, due to the polymer/gold nanoparticle interfaces.

Property	Bare Au NPs	Grafted Au NPs
Density	0.5 - 1.0 nm	1.7 - 3.0 nm
Structural	0.5 - 1.0 nm	0.5 - 1.3 nm
Local (segmental) dynamics	1.0 - 1.5 nm	0.5 - 1.5 nm
Global dynamics	3.0 - 4.0 nm	0.8 - 2.0 nm

**Table 2:** The width of the interface in PE/au NP nanocomposites defined via different properties for the systems with 100mers PE chains.

**Supplementary Materials:** The following is available online at [www.mdpi.com/xxx/s1](http://www.mdpi.com/xxx/s1), Video S1: PE-grafted AuNP. Video from MD simulation of hybrid polyethylene/grafted gold nanoparticle at 450K. Au nanoparticle (2461 atoms, diameter of 5.04 nm) and polyethylene (1200 chains, 100-mers per chain) are shown. In yellow is the Au and in grey are the edges of Au nanoparticle. In blue are the free CH<sub>2</sub> and the free CH<sub>3</sub> monomers. In red are the grafted CH<sub>2</sub> and CH<sub>3</sub> monomers.

**Author Contributions:** All authors have contributed in all parts of the present work.

**Funding:** The research work was supported by the Hellenic Foundation for Research and Innovation (HFRI) and the General Secretariat for Research and Technology (GSRT), under the HFRI PhD Fellowship grant (GA. no. 2406), by the European Union and Greek national funds through the Operational Program Competitiveness, Entrepreneurship and Innovation, under the call RESEARCH-CREATE-INNOVATE (project code:T1EDK-02746, MIS 5031809) and by the University of Crete, Grants for PhD Candidates. V.H. acknowledges support by project SimEA, funded by the European Union's Horizon 2020 research and innovation programme under grant agreement No 810660.

**Acknowledgments:** The work was supported by computational time granted from the Greek Research & Technology Network (GRNET) in the National HPC facility—ARIS under projects named MODYN-SHYPONAS and CDPPrSc. We thank Dr. A. Rissanou, Dr. P. Bačová and Dr. A. Behbahani for constructive discussions about the project. A.J.P. thanks Melita Power and Dr. E. Ieronymaki for their insightful comments.

**Conflicts of Interest:** The authors declare no conflict of interest. The funders had no role in the design of the study; in the collection, analyses, or interpretation of data; in the writing of the manuscript, or in the decision to publish the results.

## Appendix A

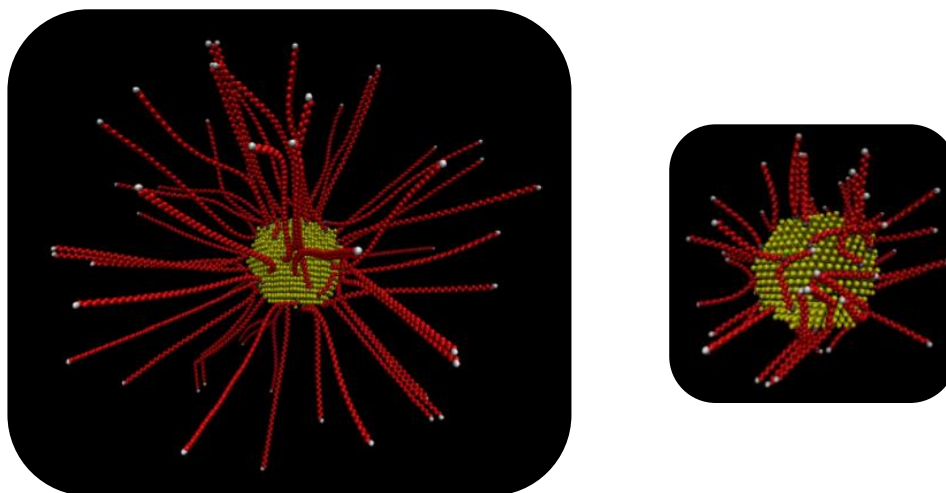


**Figure A1:** Snapshot from MD simulation of hybrid polyethylene-grafted gold nanoparticle at 450K. Au nanoparticle (2461 atoms, diameter of 5.04 nm) is shown. In yellow is the Au and in grey are the terminal CH<sub>3</sub> groups. In red are the grafted CH<sub>2</sub> and the grafted CH<sub>3</sub> monomers. The initial configuration of the grafted NP with the short anchored polymeric chains and with the long anchored polymeric chains.

### Non-Bonded Interactions

$V_{LJ}(r_{ij}) = 4\epsilon_{ij} \left[ \left( \frac{\sigma_{ij}}{r_{ij}} \right)^{12} - \left( \frac{\sigma_{ij}}{r_{ij}} \right)^6 \right], r \leq R_c$ <b style="float: right;">Lennard-Jones</b>				
Atom Types	mass (g/mol)	σ (nm)	ε (kJoule/mol)	
CH <sub>2</sub>	14.027	0.395	0.3824	
CH <sub>3</sub>	15.035	0.395	0.3824	
S - CH <sub>2</sub>	32.066 - 14.027	0.372	0.7219	
S - CH <sub>3</sub>	32.066 - 15.035	0.372	0.8761	
$V_{Morse}(r_{ij}) = D_0 [e^{-2a(r-r_0)} - 2e^{-a(r-r_0)}], r \leq R_c$ <b style="float: right;">Morse</b>				
Atom Types	mass (g/mol)	D <sub>0</sub> (kJoule/mol)	α (nm <sup>-1</sup> )	r <sub>0</sub> (nm)
Au - CH <sub>2</sub>	196.967 - 14.027	1.6885	11.69	0.4085
Au - CH <sub>3</sub>	196.967 - 15.035	1.6885	11.69	0.4085

**Table A1:** Model parameters and functional forms of all non-bonded interactions of the atomistic force field.

### Bonded Interactions

$V_b(r_{ij}) = \frac{1}{2} k_{ij}^b (r_{ij} - b_{ij})^2$				
Bond	b (nm)		k <sup>b</sup> (kJ/mol·nm <sup>2</sup> )	
CH <sub>2</sub> - CH <sub>2</sub>	0.154		100,000.00	
CH <sub>2</sub> - CH <sub>3</sub>	0.154		100,000.00	
CH <sub>3</sub> - CH <sub>2</sub>	0.154		100,000.00	
$V_\alpha(\theta_{ijk}) = \frac{1}{2} k_{ijk}^\theta (\theta_{ijk} - \theta_{ijk}^0)^2$				
Angle	θ° (deg)		k <sup>θ</sup> (kJ/mol·rad <sup>2</sup> )	
CH <sub>2</sub> - CH <sub>2</sub> - CH <sub>2</sub>	114		519.611	
CH <sub>3</sub> - CH <sub>2</sub> - CH <sub>2</sub>	114		519.611	
CH <sub>2</sub> - CH <sub>2</sub> - CH <sub>3</sub>	114		519.611	
S - CH <sub>2</sub> - CH <sub>2</sub>	114		519.611	
$V_{opls}(\varphi_{ijkl}) = \frac{1}{2} K_1 [1 + \cos(\varphi)] + \frac{1}{2} K_2 [1 - \cos(2\varphi)] + \frac{1}{2} K_3 [1 + \cos(3\varphi)] + \frac{1}{2} K_4 [1 - \cos(4\varphi)]$				
Dihedral	K <sub>1</sub> (KJ/mol)	K <sub>2</sub> (KJ/mol)	K <sub>3</sub> (KJ/mol)	K <sub>4</sub> (KJ/mol)
CH <sub>3</sub> -CH <sub>2</sub> -CH <sub>2</sub> -CH <sub>2</sub>	4.276	-1.12968	13.1545	0.00
CH <sub>2</sub> -CH <sub>2</sub> -CH <sub>2</sub> -CH <sub>2</sub>	4.276	-1.12968	13.1545	0.00
CH <sub>2</sub> -CH <sub>2</sub> -CH <sub>2</sub> -CH <sub>3</sub>	4.276	-1.12968	13.1545	0.00
S - CH <sub>2</sub> -CH <sub>2</sub> -CH <sub>2</sub>	4.276	-1.12968	13.1545	0.00

**Table A2:** Model parameters and functional forms of all bonded interactions of the atomistic force field.

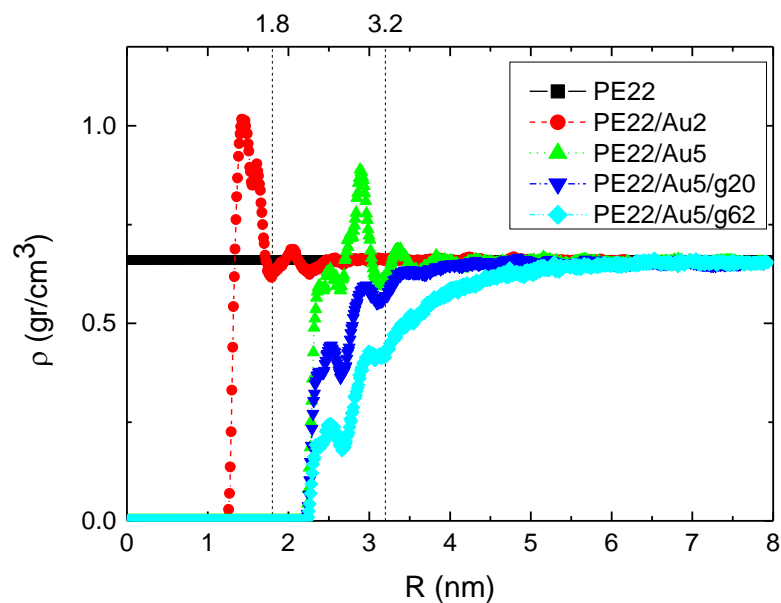


**Figure A2:** Mass monomer density profiles of polyethylene as a function of  $r$  (distance from the center of the gold NP) for the systems: PE22, PE22/Au2, PE22/Au5, PE22/Au5/g20 and PE22/Au5/g62.

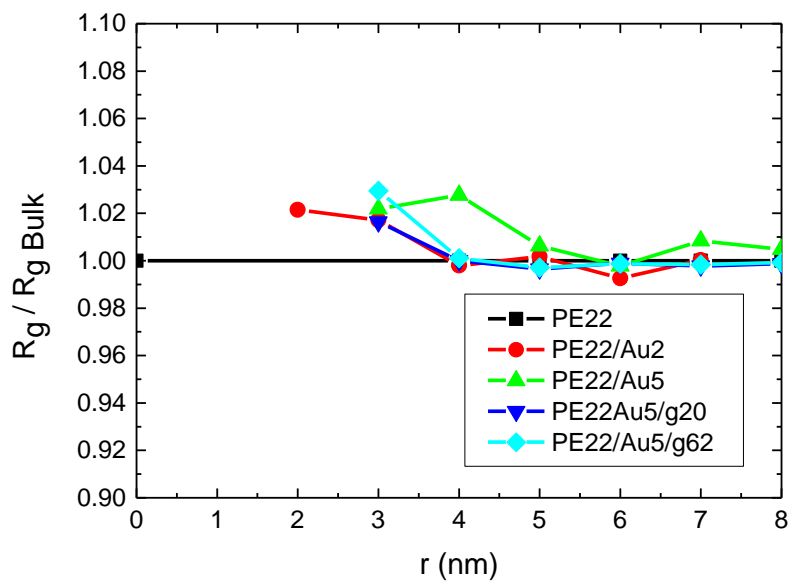


**Figure A3:** The radius of gyration ( $R_g / R_{g \text{ Bulk}}$ ) for polyethylene chains along  $R$  (distance from the center of the gold NP). Values for the PE22, PE22/Au2, PE22/Au5, PE22/Au5/g20 and PE22/Au5/g62 systems.

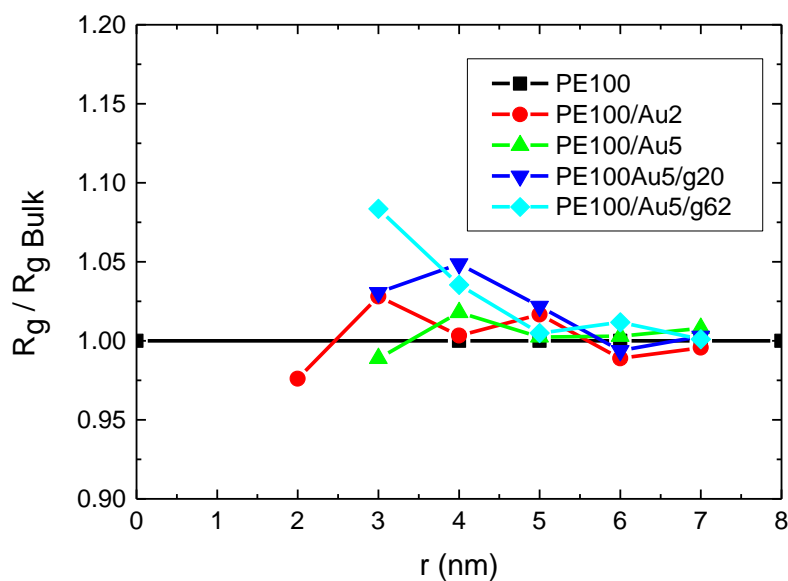


**Figure A4:** The radius of gyration ( $R_g / R_{g \text{ Bulk}}$ ) for polyethylene chains along R (distance from the center of the gold NP). Values for the PE100, PE100/Au2, PE100/Au5, PE100/Au5/g20 and PE100/Au5/g62 systems.

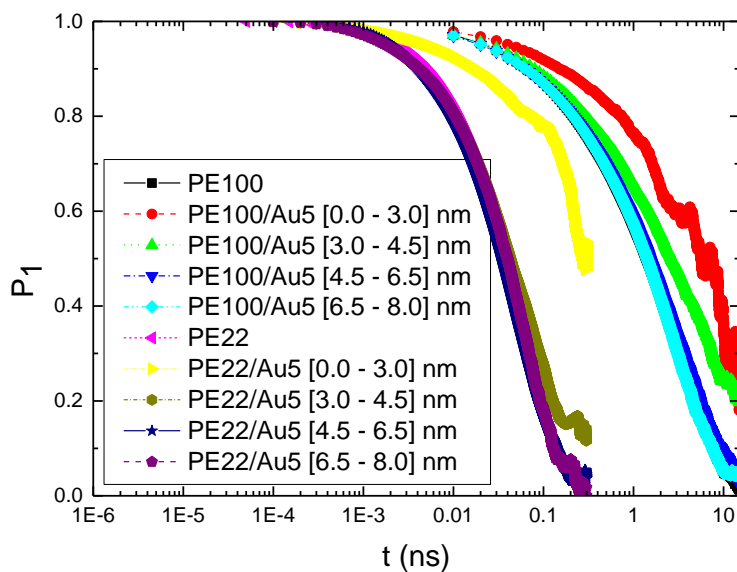


**Figure A5:** Time autocorrelation function (ACF) of bond order parameter  $P_1(t)$  as a function of time for the characteristic vector  $v^{e-e}$  of polyethylene for PE22/Au5 and PE100/Au5 systems.  $P_1(t)$  values for the PE22/Au5 and PE100/Au5 systems, for various spherical shells.

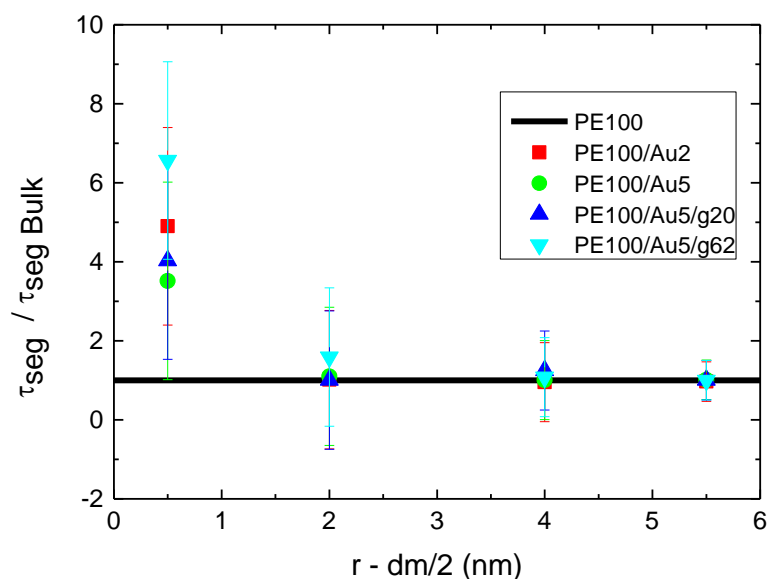


**Figure A6:** Relaxation time,  $\tau_{\text{seg}}/\tau_{\text{seg Bulk}}$ , of  $v^{1-3}$  characteristic vector based on  $P_2(t) = \frac{3}{2}\langle \cos^2\theta(t) \rangle - \frac{1}{2}$  time autocorrelation as a function of  $r$  (distance from the center of the Au NP) minus the half diameter of the NP for all systems with PE matrices consisting of 100mers per chain. Black line represents  $\tau_{\text{seg}}$  values of bulk PE under same conditions ( $T = 450$  K,  $P = 1$  atm).

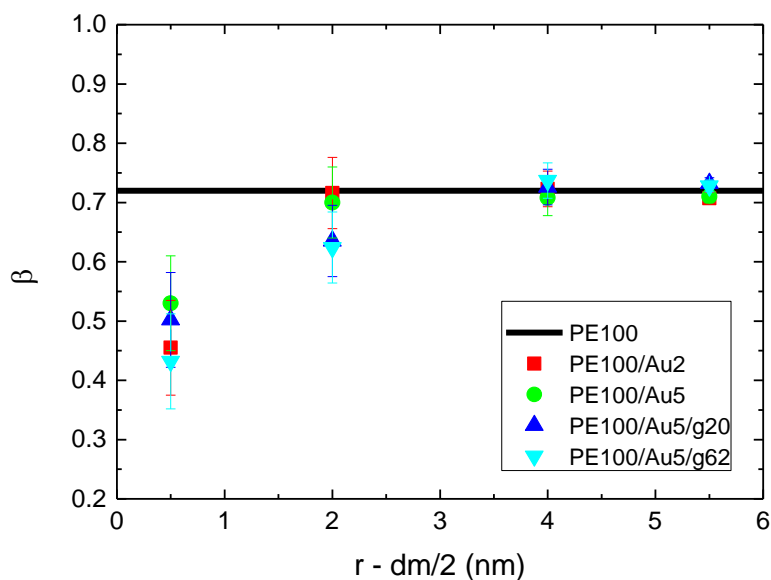


**Figure A7:** The stretch exponent  $\beta$ , as extracted from the fit with KWW functions, of  $v^{1-3}$  characteristic vector based on  $P_2(t) = \frac{3}{2}\langle \cos^2\theta(t) \rangle - \frac{1}{2}$  time autocorrelation as a function of  $r$  (distance from the center of the Au NP) minus the half diameter of the NP, for all systems with PE matrices consisting of 100mers per chain. Black lines represent  $\beta$  values of bulk PE.

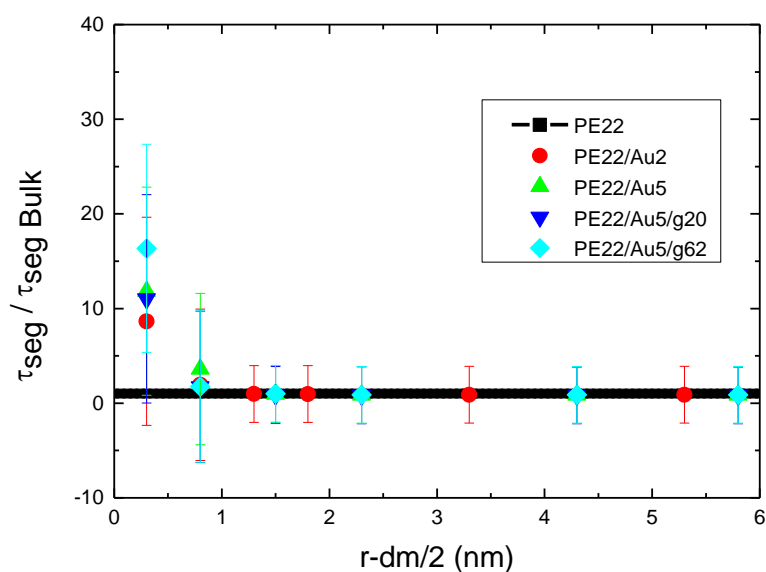


**Figure A8:** Relaxation time,  $\tau_{\text{seg}} / \tau_{\text{seg Bulk}}$ , of  $v^{1-3}$  characteristic vector based on  $P_2(t) = \frac{3}{2} \langle \cos^2 \theta(t) \rangle - \frac{1}{2}$  time autocorrelation as a function of  $r$  (distance from the center of the Au NP) minus the half diameter of the NP for all systems with PE matrices consisting of 22mers per chain. Black line represents  $\tau_{\text{seg}}$  values of bulk PE under same conditions ( $T = 450$  K,  $P = 1$  atm).

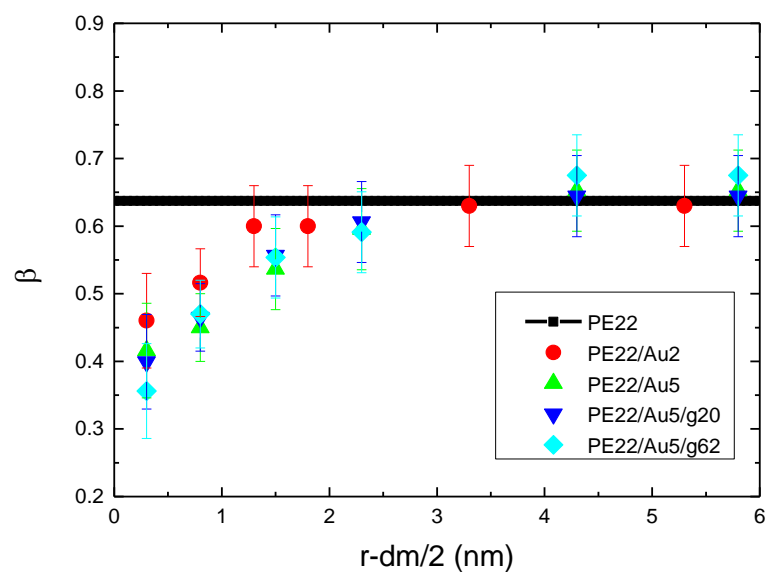


**Figure A9:** The stretch exponent  $\beta$ , as extracted from the fit with KWW functions, of  $v^{1-3}$  characteristic vector based on  $P_2(t) = \frac{3}{2} \langle \cos^2 \theta(t) \rangle - \frac{1}{2}$  time autocorrelation as a function of  $r$  (distance from the center of the Au NP) minus the half diameter of the NP, for all systems with PE matrices consisting of 22mers per chain. Black lines represent  $\beta$  values of bulk PE.

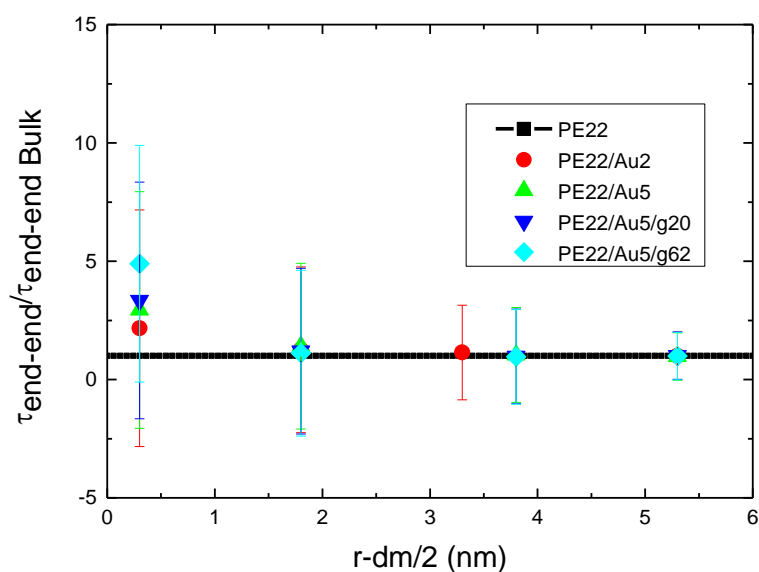


**Figure A10:** Relaxation time,  $\tau_{\text{end-end}}/\tau_{\text{end-end Bulk}}$ , of  $v^{\text{e-e}}$  characteristic vector based on  $P_1(t)$  time autocorrelation as a function of  $r$  (distance from the center of the Au NP) minus the half diameter of the NP for all systems with PE matrices consisting of 22mers per chain. Black line represents  $\tau_{\text{end-end}}$  values of bulk PE under same conditions ( $T = 450$  K,  $P = 1$  atm).

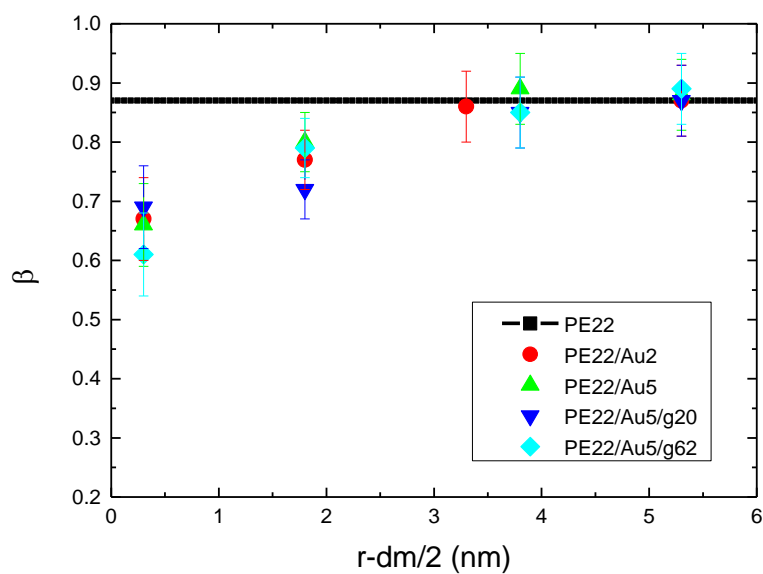


**Figure A11:** The stretch exponent  $\beta$ , as extracted from the fit with KWW functions, of  $v^{\text{e-e}}$  characteristic vector based on  $P_1(t)$  time autocorrelation as a function of  $r$  (distance from the center of the Au NP) minus the half diameter of the NP, for all systems with PE matrices consisting of 22mers per chain. Black lines represent  $\beta$  values of bulk PE.

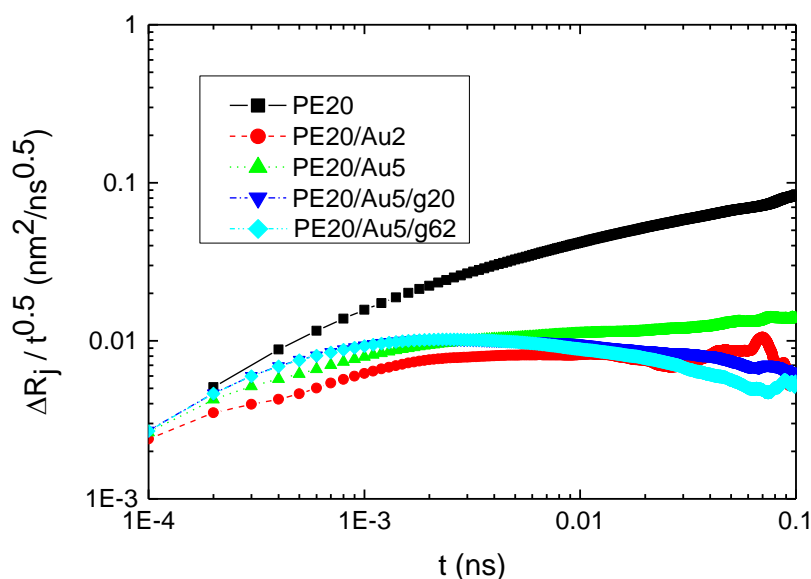


**Figure A12:** Segmental mean squared displacement for polyethylene chains along  $R$  (distance from the center of the gold NP) scaled with  $t^{0.5}$ ,  $\frac{\Delta R_j}{t^{0.5}}$ . Values for the PE22, PE22/Au2, PE22/Au5, PE22/Au5/g20 and PE22/Au5/g62 systems, for the first adsorption spherical shell of each system.

## References

1. Fu, S., et al., *Some basic aspects of polymer nanocomposites: A critical review*. Nano Materials Science, 2019. **1**(1): p. 2-30.
2. Alonso-Redondo, E., et al., *Robustness of elastic properties in polymer nanocomposite films examined over the full volume fraction range*. Scientific Reports, 2018. **8**(1): p. 16986.
3. Bačová, P., A.N. Rissanou, and V. Harmandaris, *Edge-Functionalized Graphene as a Nanofiller: Molecular Dynamics Simulation Study*. Macromolecules, 2015. **48**(24): p. 9024-9038.
4. Srivastava, S., et al., *25th Anniversary Article: Polymer-Particle Composites: Phase Stability and Applications in Electrochemical Energy Storage*. Advanced Materials, 2014. **26**(2): p. 201-234.
5. Kumar, S.K. and R. Krishnamoorti, *Nanocomposites: Structure, Phase Behavior, and Properties*. Annual Review of Chemical and Biomolecular Engineering, 2010. **1**(1): p. 37-58.
6. Giannelis, E.P., *Polymer Layered Silicate Nanocomposites*. Advanced Materials, 1996. **8**(1): p. 29-35.
7. Balazs, A.C., T. Emrick, and T.P. Russell, *Nanoparticle Polymer Composites: Where Two Small Worlds Meet*. Science, 2006. **314**(5802): p. 1107.
8. Meena Devi, J., *Aggregation of thiol coated gold nanoparticles: A simulation study on the effect of polymer coverage density and solvent*. Computational Materials Science, 2014. **86**: p. 174-179.
9. Ma, J.-z., et al., *Research advances in polymer emulsion based on "core-shell" structure particle design*. Advances in Colloid and Interface Science, 2013. **197-198**(0): p. 118-131.
10. Chrissopoulou, K., et al., *Crystallinity and Chain Conformation in PEO/Layered Silicate Nanocomposites*. Macromolecules, 2011. **44**(24): p. 9710-9722.
11. Corbierre, M.K., et al., *Gold Nanoparticle/Polymer Nanocomposites: Dispersion of Nanoparticles as a Function of Capping Agent Molecular Weight and Grafting Density*. Langmuir, 2005. **21**(13): p. 6063-6072.

12. Kotelyanskii, M. and D.N. Theodorou, *Simulation Methods for Polymers*. Marcel Dekker Inc., New York, USA, 2004.
13. Dhoke, S.K. and A.S. Khanna, *Study on electrochemical behavior of Nano-ZnO modified alkyd-based waterborne coatings*. Journal of Applied Polymer Science, 2009. **113**(4): p. 2232-2237.
14. Laachachi, A., et al., *Effect of ZnO and organo-modified montmorillonite on thermal degradation of poly(methyl methacrylate) nanocomposites*. Polymer Degradation and Stability, 2009. **94**(4): p. 670-678.
15. Dashtizadeh, A., et al., *Acrylic coatings exhibiting improved hardness, solvent resistance and glossiness by using silica nano-composites*. Applied Surface Science, 2011. **257**(6): p. 2118-2125.
16. Che, X.-C., Y.-Z. Jin, and Y.-S. Lee, *Preparation of nano-TiO<sub>2</sub>/polyurethane emulsions via in situ RAFT polymerization*. Progress in Organic Coatings, 2010. **69**(4): p. 534-538.
17. Zhu, A., et al., *Synthesis of core-shell PMMA-SiO<sub>2</sub> nanoparticles with suspension-dispersion-polymerization in an aqueous system and its effect on mechanical properties of PVC composites*. Polymer Testing, 2008. **27**(5): p. 540-547.
18. Wen, X.-f., et al., *Study of the physicochemical properties of silica powder and the stability of organic-inorganic hybrid emulsion in the presence of ethanol*. Colloids and Surfaces A: Physicochemical and Engineering Aspects, 2008. **327**(1-3): p. 103-110.
19. Kritikos, G. and K. Karatasos, *Temperature dependence of dynamic and mechanical properties in poly(acrylic acid)/graphene oxide nanocomposites*. Materials Today Communications, 2017. **13**: p. 359-366.
20. España-Sánchez, B.L., et al., *Enhanced Antibacterial Activity of Melt Processed Poly(propylene) Ag and Cu Nanocomposites by Argon Plasma Treatment*. Plasma Processes and Polymers, 2014. **11**(4): p. 353-365.
21. Firoz Babu, K., et al., *One pot synthesis of polypyrrole silver nanocomposite on cotton fabrics for multifunctional property*. Carbohydrate Polymers, 2012. **90**(4): p. 1557-1563.
22. Palza, H., *Antimicrobial Polymers with Metal Nanoparticles*. International Journal of Molecular Sciences, 2015. **16**(1): p. 2099-2116.
23. Nascimento, H.P.O., et al., *An impedimetric biosensor for detection of dengue serotype at picomolar concentration based on gold nanoparticles-polyaniline hybrid composites*. Colloids and Surfaces B: Biointerfaces, 2011. **86**(2): p. 414-419.
24. Pérez-López, A.M., et al., *Gold-Triggered Uncaging Chemistry in Living Systems*. Angewandte Chemie International Edition, 2017. **56**(41): p. 12548-12552.
25. Shevach, M., et al., *Gold Nanoparticle-Decellularized Matrix Hybrids for Cardiac Tissue Engineering*. Nano Letters, 2014. **14**(10): p. 5792-5796.
26. Ribeiro, M., et al., *Antibacterial silk fibroin/nanohydroxyapatite hydrogels with silver and gold nanoparticles for bone regeneration*. Nanomedicine: Nanotechnology, Biology and Medicine, 2017. **13**(1): p. 231-239.
27. Li, Z., et al., *Recent Advances of Using Hybrid Nanocarriers in Remotely Controlled Therapeutic Delivery*. Small, 2016. **12**(35): p. 4782-4806.
28. Bodelón, G., et al., *Au@pNIPAM SERRS Tags for Multiplex Immunophenotyping Cellular Receptors and Imaging Tumor Cells*. Small, 2015. **11**(33): p. 4149-4157.
29. Xiao, C., et al., *Responsive Au@polymer hybrid microgels for the simultaneous modulation and monitoring of Au-catalyzed chemical reaction*. Journal of Materials Chemistry A, 2014. **2**(25): p. 9514-9523.
30. Tang, F., et al., *Hybrid conjugated polymer-Ag@PNIPAM fluorescent nanoparticles with metal-enhanced fluorescence*. Journal of Materials Chemistry, 2011. **21**(42): p. 16943-16948.
31. Zhang, J., et al., *pH- and Glucose-Responsive Core-Shell Hybrid Nanoparticles with Controllable Metal-Enhanced Fluorescence Effects*. ACS Applied Materials & Interfaces, 2012. **4**(3): p. 1747-1751.

32. Tamayo, L., et al., 8 - *Polymer Composites With Metal Nanoparticles: Synthesis, Properties, and Applications*, in *Polymer Composites with Functionalized Nanoparticles*, K. Pielichowski and T.M. Majka, Editors. 2019, Elsevier. p. 249-286.
33. Ding, Y., et al., *Gold Nanoparticles for Nucleic Acid Delivery*. *Molecular Therapy*. **22**(6): p. 1075-1083.
34. Lai, C.-T., et al., *Molecular Dynamics Simulation and Experimental Studies of Gold Nanoparticle Templated HDL-like Nanoparticles for Cholesterol Metabolism Therapeutics*. *ACS Applied Materials & Interfaces*, 2017. **9**(2): p. 1247-1254.
35. Zhou, P., et al., *Reversible Regulation of Catalytic Activity of Gold Nanoparticles with DNA Nanomachines*. *Scientific Reports*, 2015. **5**: p. 14402.
36. Teranishi, T., *Fabrication and electronic properties of gold nanoparticle superlattices*. *Comptes Rendus Chimie*, 2003. **6**(8): p. 979-987.
37. Kim, Y., R.C. Johnson, and J.T. Hupp, *Gold Nanoparticle-Based Sensing of "Spectroscopically Silent" Heavy Metal Ions*. *Nano Letters*, 2001. **1**(4): p. 165-167.
38. Boisselier, E. and D. Astruc, *Gold nanoparticles in nanomedicine: preparations, imaging, diagnostics, therapies and toxicity*. *Chemical Society Reviews*, 2009. **38**(6): p. 1759-1782.
39. Lal, S., S. Link, and N.J. Halas, *Nano-optics from sensing to waveguiding*. *Nat Photon*, 2007. **1**(11): p. 641-648.
40. Lu, Y., et al., *Synthesis and Self-Assembly of Au@SiO<sub>2</sub> Core-Shell Colloids*. *Nano Letters*, 2002. **2**(7): p. 785-788.
41. Zhang, R.-C., et al., *Gold nanoparticle-polymer nanocomposites synthesized by room temperature atmospheric pressure plasma and their potential for fuel cell electrocatalytic application*. *Scientific Reports*, 2017. **7**(1): p. 46682.
42. Wang, Z., et al., *Rapid Charging of Thermal Energy Storage Materials through Plasmonic Heating*. *Scientific Reports*, 2014. **4**: p. 6246.
43. Edwardson, T.G.W., et al., *Transfer of molecular recognition information from DNA nanostructures to gold nanoparticles*. *Nature Chemistry*, 2016. **8**: p. 162.
44. Govorov, A.O., et al., *Gold nanoparticle ensembles as heaters and actuators: melting and collective plasmon resonances*. *Nanoscale Research Letters*, 2006. **1**(1): p. 84.
45. Anker, J.N., et al., *Biosensing with plasmonic nanosensors*. *Nature Materials*, 2008. **7**: p. 442.
46. Shinde, S., et al., *A Spectral Probe for Detection of Aluminum (III) Ions Using Surface Functionalized Gold Nanoparticles*. *Nanomaterials*, 2017. **7**(10): p. 287.
47. Alsawafta, M., et al., *Gold-Poly(methyl methacrylate) Nanocomposite Films for Plasmonic Biosensing Applications*. *Polymers*, 2011. **3**(4): p. 1833.
48. Betzer, O., et al., *In-vitro Optimization of Nanoparticle-Cell Labeling Protocols for In-vivo Cell Tracking Applications*. *Scientific Reports*, 2015. **5**: p. 15400.
49. Liu, M., et al., *Real-time visualization of clustering and intracellular transport of gold nanoparticles by correlative imaging*. *Nature Communications*, 2017. **8**: p. 15646.
50. Park, J.H., et al., *Polymer/Gold Nanoparticle Nanocomposite Light-Emitting Diodes: Enhancement of Electroluminescence Stability and Quantum Efficiency of Blue-Light-Emitting Polymers*. *Chemistry of Materials*, 2004. **16**(4): p. 688-692.
51. Gupta, R. and B. Rai, *Effect of Size and Surface Charge of Gold Nanoparticles on their Skin Permeability: A Molecular Dynamics Study*. *Scientific Reports*, 2017. **7**: p. 45292.
52. Ghosh, P., et al., *Gold nanoparticles in delivery applications*. *Advanced Drug Delivery Reviews*, 2008. **60**(11): p. 1307-1315.

53. Remediakis, I.N., N. Lopez, and J.K. Nørskov, *CO oxidation on gold nanoparticles: Theoretical studies*. Applied Catalysis A: General, 2005. **291**(1–2): p. 13-20.
54. Remediakis, I.N., N. Lopez, and J.K. Nørskov, *CO Oxidation on Rutile-Supported Au Nanoparticles*. Angewandte Chemie International Edition, 2005. **44**(12): p. 1824-1826.
55. Haruta, M., *4 Catalysis and applications of gold nanoparticles*, in *Studies in Surface Science and Catalysis*, M. Anpo, M. Onaka, and H. Yamashita, Editors. 2003, Elsevier. p. 31-38.
56. Von White, G., F.S. Mohammed, and C.L. Kitchens, *Small-Angle Neutron Scattering Investigation of Gold Nanoparticle Clustering and Ligand Structure Under Antisolvent Conditions*. The Journal of Physical Chemistry C, 2011. **115**(38): p. 18397-18405.
57. Jia, H., I. Grillo, and S. Titmuss, *Small Angle Neutron Scattering Study of Polyelectrolyte Brushes Grafted to Well-Defined Gold Nanoparticle Interfaces*. Langmuir, 2010. **26**(10): p. 7482-7488.
58. Jang, J.D., et al., *Self-assembly of gold nanoparticles in a block copolymer aggregate template driven by hydrophobic interactions*. Polymer Chemistry, 2019. **10**(46): p. 6269-6277.
59. Coelho, S.C., et al., *Structural characterization of functionalized gold nanoparticles for drug delivery in cancer therapy: a NMR based approach*. Physical Chemistry Chemical Physics, 2015. **17**(29): p. 18971-18979.
60. Zhou, B., et al., *Structural characterization of PEGylated polyethylenimine-entrapped gold nanoparticles: an NMR study*. Analyst, 2016. **141**(18): p. 5390-5397.
61. Guo, C. and J.L. Yarger, *Characterizing gold nanoparticles by NMR spectroscopy*. Magnetic Resonance in Chemistry, 2018. **56**(11): p. 1074-1082.
62. Farea, M.O., A.M. Abdelghany, and A.H. Oraby, *Optical and dielectric characteristics of polyethylene oxide/sodium alginate-modified gold nanocomposites*. RSC Advances, 2020. **10**(62): p. 37621-37630.
63. Mangal, R., S. Srivastava, and L.A. Archer, *Phase stability and dynamics of entangled polymer–nanoparticle composites*. Nature Communications, 2015. **6**(1): p. 7198.
64. Mijović, J., et al., *Dynamics in Polymer–Silicate Nanocomposites As Studied by Dielectric Relaxation Spectroscopy and Dynamic Mechanical Spectroscopy*. Macromolecules, 2006. **39**(6): p. 2172-2182.
65. Papadimitriou, K.D., et al., *Molecular Modeling Combined with Advanced Chemistry for the Rational Design of Efficient Graphene Dispersing Agents*. ACS Macro Letters, 2016. **5**(1): p. 24-29.
66. Monti, S., V. Caravetta, and H. Agren, *Decoration of gold nanoparticles with cysteine in solution: reactive molecular dynamics simulations*. Nanoscale, 2016. **8**(26): p. 12929-12938.
67. Ndoro, T.V.M., et al., *Interface of Grafted and Ungrafted Silica Nanoparticles with a Polystyrene Matrix: Atomistic Molecular Dynamics Simulations*. Macromolecules, 2011. **44**(7): p. 2316-2327.
68. Allen, M.P. and D.J. Tildesley, *Computer simulation of liquids*. Oxford Science, Oxford, 1987.
69. Doi, M. and S.F. Edwards, *The Theory of Polymer Dynamics*. Clarendon: Oxford, 1986.
70. Karatasos, K., *Self-Association and Complexation of the Anti-Cancer Drug Doxorubicin with PEGylated Hyperbranched Polyesters in an Aqueous Environment*. The Journal of Physical Chemistry B, 2013. **117**(8): p. 2564-2575.
71. Harmandaris, V.A., et al., *Atomistic molecular dynamics simulation of diffusion in binary liquid n-alkane mixtures*. The Journal of Chemical Physics, 2002. **116**(17): p. 7656.
72. Milano, G., et al., *Gold Nanoparticle/Polymer Interfaces: All Atom Structures from Molecular Dynamics Simulations*. The Journal of Physical Chemistry C, 2011. **115**(31): p. 15154-15163.
73. Rissanou, A.N., et al., *Structural and Conformational Properties of Poly(ethylene oxide)/Silica Nanocomposites: Effect of Confinement*. Macromolecules, 2017. **50**(16): p. 6273-6284.
74. Fotiadou, S., et al., *Structure and Dynamics of Hyperbranched Polymer/Layered Silicate Nanocomposites*. Macromolecules, 2013. **46**(7): p. 2842-2855.

75. Binder, K., *Monte Carlo and Molecular Dynamics Simulations in Polymer Science*. Oxford University Press: New York, 1995.
76. Vogiatzis, G.G. and D.N. Theodorou, *Structure of Polymer Layers Grafted to Nanoparticles in Silica–Polystyrene Nanocomposites*. *Macromolecules*, 2013. **46**(11): p. 4670-4683.
77. Tsourtou, F.D., et al., *Atomistic Monte Carlo and molecular dynamics simulation of the bulk phase self-assembly of semifluorinated alkanes*. *Chemical Engineering Science*, 2015. **121**: p. 32-50.
78. Ginzburg, V.V., *Polymer-Grafted Nanoparticles in Polymer Melts: Modeling Using the Combined SCFT–DFT Approach*. *Macromolecules*, 2013. **46**(24): p. 9798-9805.
79. Posel, Z., et al., *Highly grafted polystyrene/polyvinylpyridine polymer gold nanoparticles in a good solvent: effects of chain length and composition*. *Soft Matter*, 2016. **12**(15): p. 3600-3611.
80. Lin, J., et al., *PEGylation on mixed monolayer gold nanoparticles: Effect of grafting density, chain length, and surface curvature*. *Journal of Colloid and Interface Science*, 2017. **504**: p. 325-333.
81. Hagita, K., et al., *Coarse-Grained Molecular Dynamics Simulation of Filled Polymer Nanocomposites under Uniaxial Elongation*. *Macromolecules*, 2016. **49**(5): p. 1972-1983.
82. Patra, T.K. and J.K. Singh, *Coarse-grain molecular dynamics simulations of nanoparticle-polymer melt: Dispersion vs. agglomeration*. *The Journal of Chemical Physics*, 2013. **138**(14): p. 144901.
83. Quan, X., et al., *Structural properties of polymer-brush-grafted gold nanoparticles at the oil-water interface: insights from coarse-grained simulations*. *Soft Matter*, 2016. **12**(14): p. 3352-3359.
84. Matsuda, T., et al., *Stochastic Dynamics Simulations of n-Alkane Melts Confined between Solid Surfaces: Influence of Surface Properties and Comparison with Scheutjens-Fleer Theory*. *Macromolecules*, 1995. **28**(1): p. 165-173.
85. Johnston, K. and V. Harmandaris, *Hierarchical simulations of hybrid polymer–solid materials*. *Soft Matter*, 2013. **9**(29): p. 6696-6710.
86. Johnston, K. and V. Harmandaris, *Hierarchical Multiscale Modeling of Polymer–Solid Interfaces: Atomistic to Coarse-Grained Description and Structural and Conformational Properties of Polystyrene–Gold Systems*. *Macromolecules*, 2013. **46**(14): p. 5741-5750.
87. Priestley, R.D., et al., *Structural relaxation of polymer glasses at surfaces, interfaces, and in between*. *Science*, 2005. **309**(5733): p. 456-9.
88. Harmandaris, V.A., K.C. Daoulas, and V.G. Mavrantzas, *Molecular Dynamics Simulation of a Polymer Melt/Solid Interface: Local Dynamics and Chain Mobility in a Thin Film of Polyethylene Melt Adsorbed on Graphite*. *Macromolecules*, 2005. **38**(13): p. 5796-5809.
89. Daoulas, K.C., V.A. Harmandaris, and V.G. Mavrantzas, *Detailed Atomistic Simulation of a Polymer Melt/Solid Interface: Structure, Density, and Conformation of a Thin Film of Polyethylene Melt Adsorbed on Graphite*. *Macromolecules*, 2005. **38**(13): p. 5780-5795.
90. Anastasiadis, S.H., et al., *Nanoscale-confinement effects on local dynamics*. *Phys Rev Lett*, 2000. **84**(5): p. 915-8.
91. Johnson, K. and V. Harmandaris, *Properties of short polystyrene chains confined between two gold surfaces through a combined density functional theory and classical molecular dynamics approach*. *Soft Matter*, 2012. **8**: p. 6320-6332
92. Mischler, C., et al., *Structure and dynamics of thin polymer films: a case study with the bond-fluctuation model*. *Polymer*, 2002. **43**(2): p. 467-476.
93. Aoyagi, T., J.-i. Takimoto, and M. Doi, *Molecular dynamics study of polymer melt confined between walls*. *The Journal of Chemical Physics*, 2001. **115**(1): p. 552-559.

94. Rissanou, A., A. Power, and V. Harmandaris, *Structural and Dynamical Properties of Polyethylene/Graphene Nanocomposites through Molecular Dynamics Simulations*. *Polymers*, 2015. **7**(3): p. 390-417.
95. Martin, T.B. and A. Jayaraman, *Using Theory and Simulations To Calculate Effective Interactions in Polymer Nanocomposites with Polymer-Grafted Nanoparticles*. *Macromolecules*, 2016. **49**(24): p. 9684-9692.
96. Ge, T., G.S. Grest, and M. Rubinstein, *Nanorheology of Entangled Polymer Melts*. *Physical Review Letters*, 2018. **120**(5): p. 057801.
97. Peters, B.L., et al., *Coarse-Grained Modeling of Polyethylene Melts: Effect on Dynamics*. *Journal of Chemical Theory and Computation*, 2017. **13**(6): p. 2890-2896.
98. Nodoro, T.V.M., M.C. Böhm, and F. Müller-Plathe, *Interface and Interphase Dynamics of Polystyrene Chains near Grafted and Ungrafted Silica Nanoparticles*. *Macromolecules*, 2012. **45**(1): p. 171-179.
99. Sgouros, A.P. and D.N. Theodorou, *Atomistic simulations of long-chain polyethylene melts flowing past gold surfaces: structure and wall-slip*. *Molecular Physics*, 2020: p. 1-20.
100. Jabbarzadeh, A., J.D. Atkinson, and R.I. Tanner, *Nanorheology of molecularly thin films of n-hexadecane in Couette shear flow by molecular dynamics simulation*. *Journal of Non-Newtonian Fluid Mechanics*, 1998. **77**(1): p. 53-78.
101. Berro, H., et al., *Energy dissipation in non-isothermal molecular dynamics simulations of confined liquids under shear*. *The Journal of Chemical Physics*, 2011. **135**(13): p. 134708.
102. Bright, K., B.W. Malpass, and D.E. Packham, *Adhesion of Polyethylene to Metals*. *Nature*, 1969. **223**: p. 1360.
103. Suresh, B., et al., *Mechanical and surface properties of low-density polyethylene film modified by photo-oxidation*. *Polymer Journal*, 2011. **43**: p. 398.
104. Song, H., et al., *Migration of silver from nanosilver-polyethylene composite packaging into food simulants*. *Food Additives & Contaminants: Part A*, 2011. **28**(12): p. 1758-1762.
105. Rissanou, A. and V. Harmandaris, *Dynamics of Polymer/Graphene Interfacial Systems*. *Soft Matter*, 2014. **10**: p. 2876-2888.
106. Hautman, J. and M.L. Klein, *Simulation of a monolayer of alkyl thiol chains*. *The Journal of Chemical Physics*, 1989. **91**(8): p. 4994-5001.
107. Barmparis, G.D., K. Honkala, and I.N. Remediakis, *Thiolate adsorption on Au(hkl) and equilibrium shape of large thiolate-covered gold nanoparticles*. *The Journal of Chemical Physics*, 2013. **138**(6): p. 064702.
108. Barmparis, G.D. and I.N. Remediakis, *Dependence on CO adsorption of the shapes of multifaceted gold nanoparticles: A density functional theory*. *Phys. Rev. B*, 2012. **86**(085457).
109. Rissanou, A.N. and V. Harmandaris, *Structural and Dynamical Properties of Polystyrene Thin Films Supported by Multiple Graphene Layers*. *Macromolecules*, 2015. **48**(8): p. 2761-2772.
110. Plimpton, S., *Fast Parallel Algorithms for Short-Range Molecular Dynamics*. *J Comp Phys*, 1995. **117**: p. 1-19.
111. Alexiadis, O., et al., *Atomistic Simulation of Alkanethiol Self-Assembled Monolayers on Different Metal Surfaces via a Quantum, First-Principles Parametrization of the Sulfur-Metal Interaction*. *J. Phys. Chem. C*, 2007. **111**.
112. Barmparis, G.D., et al., *Nanoparticle shapes by using Wulff constructions and first-principles calculations*. *Beilstein Journal of Nanotechnology*, 2015. **6**: p. 361-368.
113. Billinge, S.J.L. and I. Levin, *The Problem with Determining Atomic Structure at the Nanoscale*. *Science*, 2007. **316**(5824): p. 561.

114. Hadjisavvas, G., I.N. Remediakis, and P.C. Kelires, *Shape and faceting of Si nanocrystals embedded in  $\alpha$ -SiO<sub>2</sub>: A Monte Carlo study*. Physical Review B, 2006. **74**(16): p. 165419.
115. Herring, C., *Some Theorems on the Free Energies of Crystal Surfaces*. Physical Review, 1951. **82**(1): p. 87-93.
116. Vilé, G., et al., *Silver Nanoparticles for Olefin Production: New Insights into the Mechanistic Description of Propyne Hydrogenation*. ChemCatChem, 2013. **5**(12): p. 3750-3759.
117. Li, Q., et al., *Shape control in concave metal nanoparticles by etching*. Nanoscale, 2017. **9**(35): p. 13089-13094.
118. Turzi, S.S., *On the Cartesian definition of orientational order parameters*. J. Math. Phys., 2011. **52**.
119. Sgouros, A.P., et al., *Multiscale Simulations of Graphite-Capped Polyethylene Melts: Brownian Dynamics/Kinetic Monte Carlo Compared to Atomistic Calculations and Experiment*. Macromolecules, 2019. **52**(19): p. 7503-7523.
120. Gulde, M., et al., *Dynamics and Structure of Monolayer Polymer Crystallites on Graphene*. Nano Letters, 2016. **16**(11): p. 6994-7000.
121. Williams, G. and D.C. Watts, *Non-symmetrical dielectric relaxation behaviour arising from a simple empirical decay function*. Trans. Faraday Soc., 1970. **66**(80-85).
122. Harmandaris, V.A., V.G. Mavrantzas, and D.N. Theodorou, *Atomistic Molecular Dynamics Simulation of Polydisperse Linear Polyethylene Melts*. Macromolecules, 1998. **31**(22): p. 7934-7943.
123. Harmandaris, V.A., et al., *Crossover from the Rouse to the Entangled Polymer Melt Regime: Signals from Long, Detailed Atomistic Molecular Dynamics Simulations, Supported by Rheological Experiments*. Macromolecules, 2003. **36**(4): p. 1376-1387.
124. Paul, W., G.D. Smith, and D.Y. Yoon, *Static and Dynamic Properties of a n-C100H202 Melt from Molecular Dynamics Simulations*. Macromolecules, 1997. **30**(25): p. 7772-7780.